Investigating motor and neuromuscular junction defects in a zebrafish Stathmin-2 knockout model

Tyler J.N. Gurberg

Integrated Program in Neuroscience
McGill University

April 2024

A thesis submitted to McGill University in partial fulfillment of the requirements of the degree of *Master of Science*

Table of Contents

ABSTRACT **3**

RESUME **5**

ACKNOWLEDGEMENTS **7**

AUTHOR CONTRIBUTIONS **9**

ABBREVIATION LIST **10**

LIST OF FIGURES AND TABLES **12**

RATIONALE, AIMS, AND HYPOTHESIS **13**

1. BACKGROUND KNOWLEDGE AND REVIEW OF RELEVANT LITERATURE **15**

1.1 AMYOTROPHIC LATERAL SCLEROSIS 15
1.1.1 Description of amyotrophic lateral sclerosis 15
1.1.2 ALS treatments 16
1.1.3 Genetics behind ALS. 18
1.1.4 TDP-43 proteinopathy 20
1.2 STATHMIN-2 21
1.2.1 General structure of STMN2 21
1.2.2 Function of STMN2 22
1.2.3 The cryptic exon and regulation by TDP-43 23
1.2.4 STMN2 and axon regeneration 25
1.3 ANIMAL MODELS OF STMN2 25
1.3.1 TDP-43 regulation of STMN2 in animal models 25
1.3.2 STMN2 knockout and lethality 26
1.3.3 Mouse models of STMN2 26
1.3.4 Zebrafish stmn2 28

2. MATERIALS AND METHODS **31**

3. RESULTS **38**

4. DISCUSSION AND CONCLUSION **54**

4.1 DISCUSSION 54
4.2 CONCLUSION 62

5. SUPPLEMENTARY FIGURES **64**

6. BIBLIOGRAPHY **68**

Abstract

Amyotrophic lateral sclerosis (ALS) is a progressive and fatal neurodegenerative disease characterized by the deterioration of upper and lower motor neurons, leading to paralysis. Most patients succumb to respiratory failure within 2-5 years of clinical diagnosis, and current treatments provide a modest effect on patient survival and quality of life. In 97% of ALS cases, there is cytoplasmic mislocalization of the TAR DNA Binding Protein 43 kDa (TDP-43), a protein with a significant role in regulating RNA pathways. Stathmin-2 (STMN2), a protein with a role in microtubule dynamics, has recently emerged as a misregulated downstream target of TDP-43 in ALS patients. Reduced levels of full length STMN2 and increased production of a truncated and non-functional form of the protein have been observed in patient spinal motor neurons.

This thesis explores the development and preliminary characterization of a novel animal model of STMN2 knock-out (KO). STMN2 is represented by two genes in the zebrafish genome, *stmn2a* and *stmn2b*, both of which are 74% identical and 88% similar to human *STMN2.* Using the CRISPR/Cas9 mutagenic system, we have developed the first zebrafish *stmn2a*$^{-/-}$*, stmn2b*$^{-/-}$*,* double *stmn2a*$^{-/-}$*; stmn2b*$^{-/-}$*;* and double *stmn2a*$^{-/-}$*; stmn2b*$^{-/-}$*;* Tg[*Hb9:GFP*] knock-out models. We have observed reduced survival and an early spinal curvature for double *stmn2a/b* KOs and a trend towards *stmn2a* being more important than *stmn2b*. In agreement with mouse models of STMN2 KO, we have observed a significant decrease in larval motor function in all zebrafish *stmn2* KO models as well as neuromuscular junction colocalization defects in *stmn2a*$^{-/-}$ and double *stmn2a*$^{-/-}$; *stmn2b*$^{-/-}$ models. Anecdotal evidence suggests *stmn2* may be necessary for efficient ventral root projection degeneration and subsequent regeneration following *in vivo* axotomy.

The study of ALS pathogenesis and underlying protein pathways depends largely on the study of animal models, and we believe our novel zebrafish *stmn2* KO models will contribute to our understanding of stathmin-2's role in ALS, as well as provide a model for future investigations into therapeutics targeting cytoskeletal dynamics and the *STMN2* transcript.

Résumé

La sclérose latérale amyotrophique (SLA) est une maladie neurodégénérative progressive et mortelle caractérisée par la détérioration des motoneurones supérieurs et inférieurs, résultant en paralysie. La majorité des patients succombent à l'insuffisance respiratoire dans les 2 à 5 ans suivant le diagnostic clinique, et les traitements disponibles n'ont pas grand effet sur la survie et la qualité de vie des patients. Dans 97% des cas de SLA, il y a localisation cytoplasmique de la protéine de liaison à l'ARN *TAR-DNA Binding Protein 43 kDa* (TDP-43). Cette protéine est normalement située dans le noyau cellulaire, où elle à des rôles importants dans la régulation des voies de l'ARN. Stathmin-2 (STMN2), une protéine jouant un rôle dans la dynamique des microtubules, est récemment apparue comme une cible du TDP-43 qui est mal régulée chez les patients atteints du SLA. Des niveaux réduits de STMN2 complet et une production accrue d'une forme tronquée et non fonctionnelle de la protéine ont été observés dans les motoneurones spinaux des patients.

Cette thèse explore le développement et la caractérisation préliminaire d'un nouveau modèle animal de *knock-out* (KO) de STMN2. STMN2 est représenté par deux gènes dans le génome du poisson zèbre, *stmn2a* et *stmn2b*, tous deux identiques à 74% et similaires à 88% au STMN2 humain. En utilisant le système mutagène CRISPR/Cas9, nous avons développé le premier modèle de poisson zèbre *stmn2a*$^{-/-}$, *stmn2b*$^{-/-}$, double *stmn2a*$^{-/-}$; *stmn2b*$^{-/-}$; et double *stmn2a*$^{-/-}$; *stmn2b*$^{-/-}$; Tg[*Hb9:GFP*]. Nous avons observé une survie réduite et une courbure vertébrale précoce pour les poissons zèbre doubles *stmn2a*$^{-/-}$; *stmn2b*$^{-/-}$ et une tendance vers *stmn2a* étant plus importante que *stmn2b*. En accord avec les modèles murins de STMN2 KO, nous avons observé une diminution significative de la fonction motrice des larves dans tous les modèles de poisson zèbre *stmn2* KO ainsi que des défauts de colocalisation des jonctions

neuromusculaires dans les modèles *stmn2a*$^{-/-}$ et double *stmn2a*$^{-/-}$; *stmn2b*$^{-/-}$. Des preuves anecdotiques *in vivo* suggèrent que *stmn2* pourrait être nécessaire pour une dégénérescence efficace des projections de racines ventrales et pour la régénération qui suit après une blessure axonale.

L'étude de la pathogenèse de la SLA et des voies protéiques sous-jacentes dépend en grande partie de l'étude de modèles animaux, et nous pensons que nos nouveaux modèles poisson zèbre de *stmn2* KO contribueront à notre compréhension du rôle de stathmin-2 dans la SLA, ainsi qu'à fournir un modèle pour de futures recherches sur des thérapeutiques ciblant la dynamique du cytosquelette et le STMN2.

Acknowledgements

I would like to start off by thanking the members of my lab for their continuous support during my time in the Armstrong research group. Thank you to Ziyaan, forever my office partner, and Christian, my athletic counterpart, for the training, troubleshooting, and general help they provided me and my experiments. More importantly, thank you for being incredible friends since the day I showed up to our lab. Thank you to Olivia for being an uplifting, light, and fun presence both inside and outside the lab. Thank you to Virginie for being an incredible source of knowledge and hilarious under-her-breath commentary on her own experiments, always bringing a smile to our faces. Huge thank you to Esteban, our lab manager and research assistant, for being the engine that keeps our lab running. Your eye for detail and unwavering work ethic are exemplary; any lab would be lucky to have someone like you. Finally, thank you to Dr. Gary Armstrong for being an incredible mentor and supervisor. Your passion for science and excitement over our discoveries is constantly motivating and uplifting, and I have no doubt this research group will continue to produce high-quality data under your leadership.

I would like to thank the other research groups of the sixth floor of the Montreal Neurological Institute and Hospital for their friendship and scientific curiousity, helping to push each other towards the goal of ground-breaking discoveries. Thank you to my advisory committee, Dr. Thomas Durcan and Dr. Alyson Fournier, and my mentor, Dr. Janine Mendola, for their invaluable input and guidance throughout my project. I am forever grateful for my time working at this prestigious institution, and genuinely believe McGill University to be a dream location for the brightest minds to conduct ground-breaking research.

Thank you to my parents, Richard Gurberg and Tanya Nouwens, for making me feel loved and supported every day. I would not be where I am today without having role models as amazing as you, and I hope to provide my future children with as much guidance, encouragement, and love as you have given me. Thank you to my grandfather, David Gurberg, for the continuous love and support you have provided me throughout my education. Thank you to my long-term girlfriend, Stephanie Gauron, for being the most incredible partner I could have ever dreamed of. Long days in the lab feel a lot shorter when I get to come home to you. I would not be who I am today without your (and Daisy's) love. Last, and most certainly not least, thank you to Zachary Gurberg, my beloved brother. No words can describe the love I have for you. You are an incredible man, a personal role model, and the best friend I could ever ask for. You are, and always will be, my hero.

In loving memory of Arleen Gurberg.

Author contributions

Tyler Gurberg planned and executed the experiments under the supervision of Dr. Gary Armstrong and with the support of his advisory committee, Dr. Thomas Durcan and Dr. Alyson Fournier. Tyler Gurberg drafted this Thesis, which was reviewed by Dr. Armstrong. Esteban Rodriguez Pinto performed the described *in vitro* fertilization experiments, and Dr. Armstrong helped with microinjections. Ziyaan Harji, Christian Rampal, Virginie Petel-Légaré, and Dr. Armstrong provided training on experimental protocols.

Abbreviation list

Abbreviation	Meaning
°C	degree Celsius
aBtx	alpha-bungarotoxin
ALS	amyotrophic lateral sclerosis
ALSFRS-R	revised ALS functional rating scale
ASO	antisense oligonucleotide
BAC	bacterial artificial chromosome
bp	base pairs
C9ORF72	chromosome 9 open reading frame 72
cDNA	complementary DNA
CRISPR	clustered regularly interspaced short palindromic repeats
CSF	cerebrospinal fluid
DNA	deoxyribonucleic acid
dpf	days post fertilization
ER	endoplasmic reticulum
fALS	familial amyotrophic lateral sclerosis
FTD	frontotemporal dementia/degeneration
FUS	fused in sarcoma
gapdh	glyceraldehyde-3-phosphate dehydrogenase
GFP	green fluorescent protein
gRNA	guide ribonucleic acid
GWAS	genome-wide association studies
hMN	human motor neuron
hpf	hours post fertilization
HRM	high resolution melting
iPSC	induced pluripotent stem cell
JNK1	Jun-N-terminal kinase 1
kDa	kilodalton
KO	knockout

LOF	loss-of-function
mg	milligram
mL	millilitre
MNI	Montreal neurological institute
mRNA	messenger ribonucleic acid
NfL	neurofilament light
ng	nanogram
nL	nanolitre
NMJ	neuromuscular junction
PAM	protospacer-adjacent motif
PCR	polymerase chain reaction
PBS	phosphate-buffered saline
PFA	paraformaldehyde
qRT-PCR	quantitative real-time PCR
RNA	ribonucleic acid
ROS	reactive oxygen species
RT	room temperature
sALS	sporadic amyotrophic lateral sclerosis
SCG10	superior cervical ganglion 10
SOD1	superoxide dismutase 1
STMN2	stathmin-2
Syt2	synaptotagmin 2
TBK1	TANK-binding kinase 1
TDP-43 / TARDBP	TAR DNA-binding protein 43
TL	Tübingen long fin
µg	microgram
µL	microlitre
WES	whole exome sequencing
WT	wild type

List of Figures and Tables

Figure 1 | Timeline of discovery of over 40 ALS-linked genes

Figure 2 | Schematic representation of STMN2

Figure 3 | STMN2 amino acid sequence comparison

Figure 4 | Generation and RT-qPCR analysis of *stmn2a* and *stmn2b* KO zebrafish lines

Figure 5 | Genotypic frequencies of adult zebrafish and larval morphology comparison

Figure 6 | Adult morphology comparison and *stmn2* KO spinal curvature

Figure 7 | 2 dpf touch-evoked motor response assay

Figure 8 | Neuromuscular junction abnormalities

Figure 9 | Axon regeneration following injury at 3 dpf and regeneration at 4 dpf

Supplementary Figure 1 | Restriction enzyme fragment-length polymorphism for *stmn2a* and *stmn2b*

Supplementary Figure 2 | Expected and actual observed genotypic ratios from 295 screened adult zebrafish

Supplementary Figure 3 | Example images of neuromuscular junction colocalization for wild type, *stmn2a*$^{-/-}$, *stmn2b*$^{-/-}$, and double *stmn2a*$^{-/-}$; *stmn2b*$^{-/-}$ 2 dpf larvae

Rationale, Aims, and Hypothesis

Amyotrophic lateral sclerosis (ALS) is a progressive and fatal neurodegenerative disease characterized by the degeneration of both upper and lower motor neurons. Very few treatment options are available to the roughly 1,000 Canadians that are diagnosed every year, and no cure exists. In 97% of ALS cases, there is cytoplasmic mislocalization of TAR DNA-binding protein 43 (TDP-43), a protein with a significant role in RNA metabolism that is normally located in the nucleus. Stathmin-2 has recently emerged as an important cellular target of TDP-43, as a pair of studies published in 2019 discovered that *STMN2* expression is significantly reduced in response to TDP-43 depletion (Klim et al., 2019; Melamed et al., 2019). The *STMN2* gene contains a cryptic exon whose expression is attenuated under normal conditions but, in ALS cases, results in the production of a truncated and non-functional *STMN2* variant. Neither zebrafish nor murine models contain this cryptic exon, yet the use of these model organisms allows for the study of the consequences of *STMN2* knockout independent from TDP-43 regulation. The development of novel animal models remains a critical tool for researchers investigating mechanisms of neurodegeneration and for the development of therapeutics to treat ALS.

While multiple mouse Stathmin-2 loss-of-function models have been described, no zebrafish models of *stmn2* knockout (KO) have been reported in the literature. My project seeks to develop and characterize a novel zebrafish *stmn2* KO model, contributing to our understanding of STMN2's role in maintaining motor axon projections to neuromuscular junctions (NMJs). The results of this project and the model I have developed contributes to our understanding of STMN-related motor deficits and provides a model for future drug screens targeting the modulation of microtubule networks.

AIM 1: Generation of a CRISPR KO line of zebrafish *stmn2*

I hypothesize that gRNA-target CRISPR/Cas9 microinjections will efficiently generate viable *stmn2a*$^{-/-}$, *stmn2b*$^{-/-}$, and double *stmn2a*$^{-/-}$*; stmn2b*$^{-/-}$ zebrafish models.

AIM 2: Investigate larval motor deficits in *stmn2a* KO, *stmn2b* KO, and double *stmn2a; stmn2b* KO zebrafish models

I hypothesize *stmn2a*$^{-/-}$*, stmn2b*$^{-/-}$ and double *stmn2a*$^{-/-}$*; stmn2b*$^{-/-}$ zebrafish larvae will present reduced motor function when compared to wild type animals.

AIM 3: Investigate neuromuscular junction defects in *stmn2a* KO, *stmn2b* KO, and double *stmn2a; stmn2b* KO zebrafish models

I hypothesize *stmn2a*$^{-/-}$*, stmn2b*$^{-/-}$ and double *stmn2a*$^{-/-}$*; stmn2b*$^{-/-}$ zebrafish larvae will present reduced neuromuscular junction innervation and an increase in orphaned pre- and post-synaptic terminals when compared to wild type animals.

AIM 4: Investigating the regenerative capacity of injured ventral root axon projections in a double *stmn2a; stmn2b* KO zebrafish model

I hypothesize double *stmn2a*$^{-/-}$*; stmn2b*$^{-/-}$ zebrafish larvae will have a reduced ability to regenerate transected ventral root projections when compared to wild type animals.

1. Background knowledge and review of relevant literature

1.1 Amyotrophic lateral sclerosis

1.1.1 *Description of amyotrophic lateral sclerosis*

ALS, colloquially referred to as Lou Gehrig's disease in the United States or motor neuron disease in Europe, is a neurodegenerative disease characterized by the degeneration of upper motoneurons, located in the cerebral cortex, and lower motoneurons, located in the brainstem and spinal cord. The progressive and fatal nature of the disease results in a median survival of 2-3 years following clinical onset, with respiratory failure being the most common cause of death (Oskarsson et al., 2018; Pasinelli & Brown, 2006). The disease was first described in 1869 by French neurologist Jean Martin Charcot and has an incidence rate of approximately 2 per 100,000 person-years (Beghi et al., 2006; Kiernan et al., 2011). An estimated 1,000 Canadians die from, and are diagnosed with, ALS every year (ALS Canada).

The average age of disease onset is between 55 and 65 years of age, and men are slightly more likely to be affected than women. Clinical diagnosis is difficult and can occur up to two years following initial symptoms, which can vary on a case-by-case basis (Orsini et al., 2015). Most patients (~70%) present with limb-onset disease, which can be characterized by initial symptoms of limb weakness, spasticity, or muscle atrophy in the arms or legs. The remaining patients present with bulbar-onset disease, characterized by tongue weakness and slow, difficult speech. A small subset of patients present with rare initial symptoms such as weight loss, respiratory difficulty, or frontal lobe-type cognitive deficits (Al-Chalabi & Hardiman, 2013; Kiernan et al., 2011). Diagnosis is difficult due to a lack of definitive diagnostic tests for ALS, and typically relies on the presentation of one or more symptoms outlined above in conjunction

with ruling out other diseases that manifest similar clinical pathology to ALS such as multiple sclerosis, tumours, strokes, spinal muscular atrophy, multifocal motor neuropathy, or other neuromuscular junction disorders such as myasthenia gravis (Kiernan et al., 2011; Oskarsson et al., 2018).

Historically, researchers have debated over the origin of ALS. Some have speculated that ALS progression arises from a "dying-forward" disease mechanism, suggesting ALS is primarily a corticomotoneuronal disease where degeneration of downstream anterior horn cells is triggered through glutamate-mediated excitotoxicity. Others have suggested a "dying-back" hypothesis that proposes the disease begins at the neuromuscular junction or at the muscle cell, where a postsynaptic impairment related to the release of a motor neurotrophic hormone is lost or altered in the disease process, impairing the function of the upstream anterior horn cells (Appel, 1981; Kiernan et al., 2011). Today we recognize that ALS is a heterogeneous disease that likely incorporates elements of both central and peripheral disease mechanisms, with more significance attributed to one or the other depending on the specific mutation, proteinopathies, and symptom progressions presented by individual patients (Goyal et al., 2020).

1.1.2 *ALS treatments*

No cure is currently available to ALS patients, and traditional therapies have limited effectiveness. The first drug to be approved for ALS patients was Riluzole in 1995, a medication thought to provide a 3-4 month increase to patient lifespan through attenuation of glutamate-mediated excitotoxicity (Hebert et al., 1994; Miller et al., 2007). Edaravone, first approved in 2017, reduces oxidative stress through free radical scavenging. It has been shown to slow the

decline in scores on the ALS Functional Rating Scale (ALSFRS-R, a measure of disease severity) in a subset of patients, typically those who started taking the drug earlier in the disease progression (Cruz, 2018; Oskarsson et al., 2018; Writing & Edaravone, 2017). In 2022, Albrioza (AMX0035, Amylyx Pharmaceuticals), a combination drug of sodium phenylbutyrate (PB) and taurursodiol (TURSO), was approved for ALS patients. Albrioza aims to reduce cellular stress signals in both mitochondrial and endoplasmic reticulum (ER) pathways to prevent neuronal death, and has been shown to not only increase patient lifespan by about 6.5 months, but also slow the rate of decline in ALSFRS-R score by 25% (Johnson et al., 2022; Paganoni et al., 2022; Paganoni et al., 2021; Paganoni et al., 2020). Recent developments in personalized medicine have brought a more specialized treatment, Tofersen (Biogen), to the market for patients harbouring mutations in the superoxide dismutase 1 (*SOD1)* gene. Tofersen is an antisense oligonucleotide (ASO) that targets mutant *SOD1* mRNA for nonsense-mediated decay, preventing the toxic protein from being made. Trials investigating the drug's effectiveness are still underway, though it has been shown to reduce concentrations of SOD1 in cerebrospinal fluid (CSF) and reduce concentrations of neurofilament light chains (NfL) in patient plasma, while having an insignificant effect on slowing the rate of ALSFRS-R decline in patients (Miller et al., 2022).

All available treatments for ALS patients rely on symptom management, and while the past two years have been fruitful with two new drugs becoming available to some ALS patients, further research into the underlying mechanisms behind ALS is necessary. A more in-depth understanding of the pathophysiological fundamentals behind the disease could lead to the discovery of important biomarkers that would allow patients to be treated earlier into the disease,

the discovery of potent pharmacological targets for disease regulation, and, one day, a cure for this devastating disease.

1.1.3 *Genetics behind ALS*

ALS is divided into two major groups: sporadic ALS (sALS), which makes up approximately 90% of cases, and familial ALS (fALS), making up the remaining 10% of cases, though more recent studies suggest up to 20% of ALS cases have a family history of either ALS or FTD (frontotemporal dementia/degeneration) (Brown & Al-Chalabi, 2017; Kiernan et al., 2011). While over 40 genes have been linked to ALS, the most common genes associated to the disease are chromosome 9 open reading frame 72 (*C9ORF72*), superoxide dismutase 1 (*SOD1*), TAR DNA-binding protein 43 (*TARDBP*), fused in sarcoma (*FUS*), and TANK-binding kinase 1 (*TBK1*), together making up approximately 15% of all patients, and over 70% of fALS cases (Masrori & Van Damme, 2020; Wang et al., 2023). The rate of discovery of novel ALS-linked genes continues to increase, with powerful screening techniques such as Genome-Wide Association Studies (GWAS) and Whole Exome Sequencing (WES) leading to the discovery of 12 new genes of interest since 2016 (Wang et al., 2023) (**Fig. 1**).

Figure 1

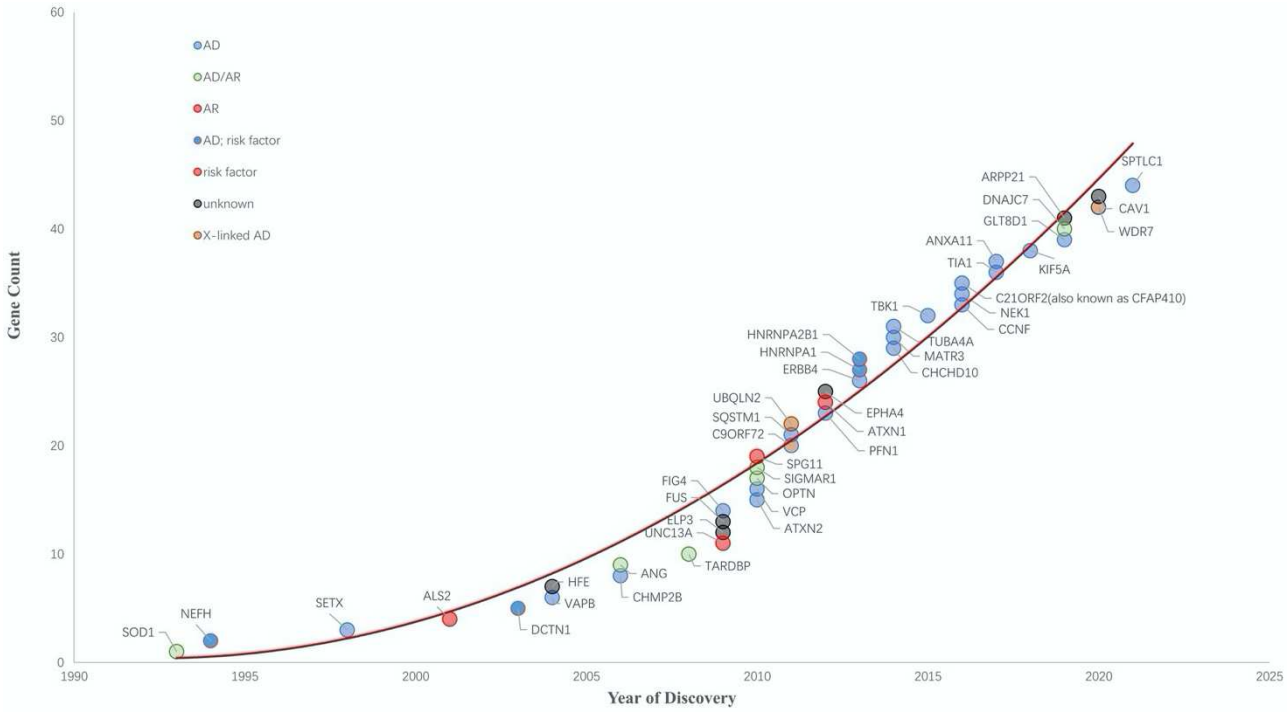

Figure 1 | Timeline of discovery of over 40 ALS-linked genes, 12 of which have resulted from modern screening techniques such as GWAS and WES since 2016. Inheritance patterns are represented by the colour of the circle. Figure taken from: (Wang et al., 2023).

Hexanucleotide repeat expansion of the "GGGGCC" sequence in *C9ORF72* is the most common genetic cause of ALS, responsible for 30-50% of fALS and 7-10% of sALS cases of European ancestry (DeJesus-Hernandez et al., 2011; Renton et al., 2011). Patients affected by mutations in *C9ORF72* typically present with reduced expression of the protein encoded by *C9ORF72*, which is associated with impairment/alteration in autophagy and inflammation (Smeyers et al., 2021). The first gene to be associated with ALS, *SOD1*, was identified in 1993 and accounts for about 20% of fALS and 5% of sALS cases (Rosen et al., 1993). Variants of

SOD1 are thought to be prone to a gain-of-toxic-function mechanism that leads to protein aggregation and disruption of its role in reducing reactive oxygen species (ROS) (Masrori & Van Damme, 2020; McCord & Fridovich, 1969; Rosen et al., 1993). Missense mutations in *TARDBP* and *FUS* and the variants of the proteins they encode result in cytoplasmic accumulation and aggregation and is thought to affect their role in RNA regulation. Mutations in these genes are thought to be responsible for 3-5% of fALS and around 1-2% of sALS cases (Kwiatkowski et al., 2009; Masrori & Van Damme, 2020; Neumann et al., 2006; Vance et al., 2009). Finally, loss-of-function mutations in *TBK1*, disrupting its role in autophagy and inflammatory pathways, is thought to be responsible for 1% of ALS patients but up to 10% of ALS-FTD patients (Cirulli et al., 2015; Le Ber et al., 2015; Masrori & Van Damme, 2020).

The overlap between ALS and FTD should be noted, as it is widely accepted that these diseases lie on the same spectrum, with clinical presentation largely depending on the extent and location of neuronal degeneration (Taylor et al., 2016). Approximately 15% of patients with ALS also meet the diagnostic criteria for FTD, and the same percentage is true for FTD patients and ALS (Ling et al., 2013; Ringholz et al., 2005). Many of the same genes outlined above (*C9ORF72, TARDBP, FUS*) also have causative links to FTD pathophysiology (Bang et al., 2015).

1.1.4 *TDP-43 proteinopathy*

TDP-43 is mostly located in the nucleus, where it has a significant role in RNA metabolism, contributing to the regulation of RNA stability, transport, and splicing (Buratti & Baralle, 2001, 2008). Immunohistochemistry and immunofluorescence experiments have been

previously performed to compare disease-affected neurons (ALS and FTD cases) to healthy ones, revealing normal, nuclear TDP-43 presence in healthy tissues whereas mislocalization from the nucleus to the cytoplasm occurs in diseased regions of the brain and spinal cord (Arai et al., 2006; Neumann et al., 2006). Despite *TARDBP* mutations making up around 5% of all ALS cases, it is estimated that nearly 97% of all ALS cases, and up to 45% of FTD cases, present with some cytoplasmic mislocalization of TDP-43 (Ling et al., 2013). While there is still debate on whether TDP-43 pathology results in a loss-of-function disease mechanism, a toxic gain-of-function mechanism, or a mix of the two, there is strong evidence that nuclear depletion of TDP-43 has a significant effect on its ability to regulate RNA pathways (Lee et al., 2011). In 2019, the Eggan and Cleveland labs investigated the effect on TDP-43 depletion on cellular mRNA levels, and both groups concluded that stathmin-2 (*STMN2*) transcripts were one of the most significantly downregulated (Klim et al., 2019; Melamed et al., 2019).

1.2 Stathmin-2

1.2.1 *General structure of STMN2*

Stathmin-2 (STMN2, formerly known as superior cervical ganglion 10 or SCG10) is made up of 179 amino acids encoded by 5 exons of the *STMN2* gene and measuring 21 kDa in weight. STMN2 is a neuronal growth-associated protein that is upregulated during development and following axonal injury, with low basal levels maintained during adulthood (Stein et al., 1988). It is located on chromosome 8 and is a member of the stathmin family of microtubule-associated phosphoproteins, which include stathmins 1 through 4. While stathmin (stathmin-1) and stathmin-3 (formerly known as SCLIP) are ubiquitously expressed in human tissues, stathmin-2 and stathmin-4 (formerly known as RB3) are highly expressed in the nervous system

(Bieche et al., 2003). All members of the stathmin-family of proteins contain a homologous C-terminal domain that includes two tubulin binding regions, a proline-rich domain that contains phosphorylation sites targeted by Jun-N-terminal Kinase 1 (JNK1), and a stathmin N-terminal domain that contains a tubulin polymerization-inhibiting peptide. *STMN2* contains a unique N-terminal domain that contains two palmytoilation sites, targeting the protein for membrane insertion in the Golgi (Benarroch, 2021; Chauvin & Sobel, 2015; Di Paolo et al., 1997).

1.2.2 *Function of STMN2*

Stathmin-2 is anterogradely trafficked to growth cones during development and following axonal injury. It is generally considered a microtubule-destabilizing protein due to its ability to sequester soluble tubulin dimers and force microtubule tip curvature, triggering microtubule depolymerization (Curmi et al., 1997; Gupta et al., 2013). Healthy microtubule networks are dynamic and undergo constant remodeling through phases of individual microtubule polymerization and depolymerization, a process known as "dynamic instability" (Mitchison & Kirschner, 1984). While the literature frequently reports STMN2 as a microtubule destabilizer due to its ability to sequester two tubulin dimers per STMN2 protein, there is evidence of differential regulation at the plus and minus ends of individual microtubules. An experiment by the Wilson group (2007) tracked individual microtubules *in vitro*, and discovered that higher concentrations of STMN2 led to not only an increased catastrophe frequency, shortening rate, and shortening length during depolymerization events at the minus end, but also an increased rate and extent of growth at the plus end (Manna et al., 2007). This differential regulation is thought to provide free, soluble tubulin from the minus end to promote plus end growth, helping

developing growth cones to advance and react to guidance cues through increased plasticity (Grenningloh et al., 2004; Manna et al., 2007).

1.2.3 *The cryptic exon and regulation by TDP-43*

STMN2 normally contains 5 exons, though a further investigation by the Eggan and Cleveland groups (2019) resulted in the discovery of a potential sixth exon located between exons 1 and 2. This cryptic exon, named exon 2a, was found to contain a premature stop codon, a premature polyadenylation sequence, as well as multiple "GU" motifs which act as TDP-43 binding sites (Klim et al., 2019; Melamed et al., 2019). In healthy individuals, nuclear TDP-43 binds to these motifs in the 2a cryptic exon, sterically blocking a 3' splice site in *STMN2* pre-mRNA and leading to normal, full-length protein production (Baughn et al., 2023). In ALS, where TDP-43 cytoplasmic mislocalization occurs in nearly all patients, nuclear TDP-43 is depleted, exposing the cryptic splice and polyadenylation sites to further RNA processing factors. The resulting truncated and non-functional protein (containing only exon 1 and the cryptic exon 2a) prevents the production of functional full-length STMN2 protein (Baughn et al., 2023) (**Fig. 2**). Indeed, RNA sequencing analysis of lumbar motor neurons from ALS patients and healthy controls indicates a significant decrease in full-length *STMN2* mRNA and an increase in truncated *STMN2* mRNA in ALS patients compared to non-ALS controls (Baughn et al., 2023; Klim et al., 2019; Melamed et al., 2019).

Figure 2

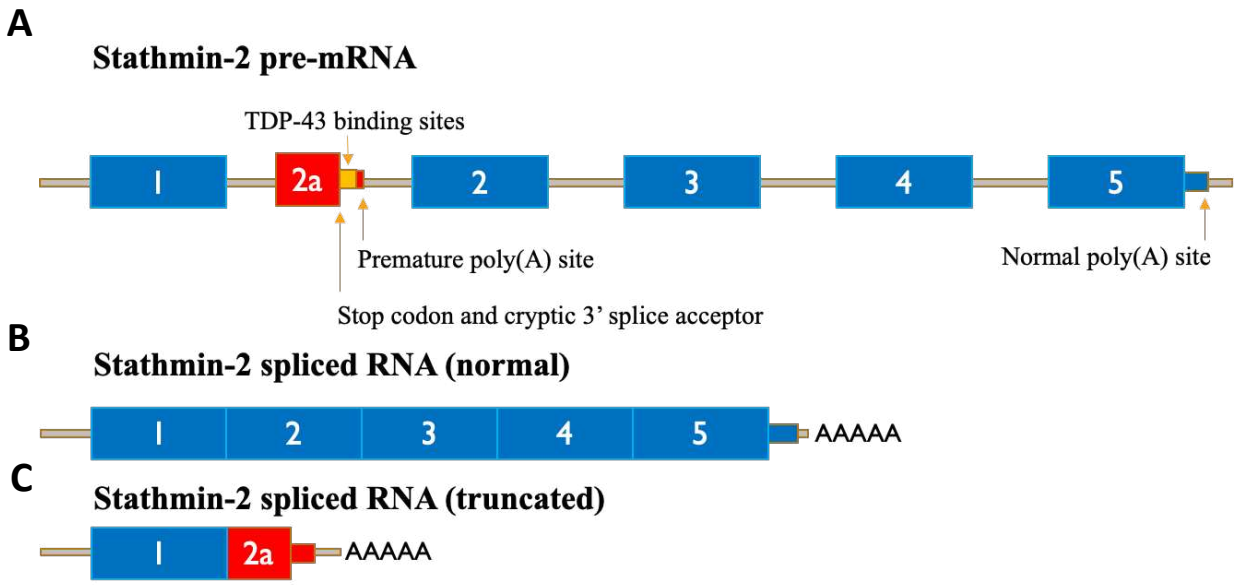

Figure 2 | Adapted and modified from Melamed et al., 2019. Schematic representation of **A**, stathmin-2 pre-mRNA, including the TDP-43 binding sites, premature stop codon, and premature polyadenylation site in the 2a cryptic exon (red). Normal exons presented in blue. **B**, normally spliced stathmin-2 RNA, as seen in healthy individuals. **C**, truncated and non-functional form of stathmin-2, as seen in ALS patients presenting TDP-43 cytoplasmic mislocalization. Nuclear depletion of TDP-43 results in exposure of a *STMN2* cryptic 3' splice site, premature stop codon, and premature polyadenylation site to RNA processing factors, preventing the production of full-length protein.

1.2.4 *STMN2 and axon regeneration*

Experiments by the Eggan and Cleveland groups (2019) investigated the role of STMN2 in axon regeneration. Human motor neurons (hMNs) or induced pluripotent stem cell (iPSC)-derived motor neurons were plated and allowed to grow axonal projections. Following axotomy, neurite regrowth was tracked, and it was discovered that cells expressing reduced levels of STMN2 had a limited ability to regrow axonal projections. Furthermore, TDP-43 depletion itself was sufficient to cause this reduced ability to regenerate axons, due to the downstream effect on STMN2 levels (Klim et al., 2019; Melamed et al., 2019). This effect could be rescued through secondary stathmin-2 transduction (Melamed et al., 2019), or through JNK1 inhibition, preventing STMN2 degradation through reduced phosphorylation of the protein (Klim et al., 2019; Tararuk et al., 2006). These experiments demonstrated that multiple mechanisms exist to potentially restore the regenerative capabilities of human motor neurons affected by STMN2 depletion, opening the door to future therapeutic options for patients with reduced levels of the STMN2 protein.

1.3 Animal models of STMN2

1.3.1 *TDP-43 regulation of STMN2 in animal models*

Despite high STMN2 amino acid conservation between human, primate, mouse, rat, and zebrafish models, the first intron, including the 2a cryptic exon, is poorly conserved beyond primates. As such, murine and zebrafish STMN2 is not regulated by TDP-43 expression. However, experiments by the Cleveland group (2023) where the 2a cryptic exon was successfully knocked into the mouse genome has shown to be sufficient to trigger cellular *Stmn2* regulation by Tdp-43 *in vitro*. Their model also presented increased production of chimeric

truncated *Stmn2* mRNA in response to Tdp-43 depletion, validating the mechanism of TDP-43 steric blocking of the cryptic 3' splice site and premature polyadenylation site (Baughn et al., 2023). The same group also demonstrated that humanized mouse cells containing the 2a cryptic exon, modified to not contain the TDP-43 binding motif, presented a nearly complete elimination of mature mouse *Stmn2* mRNA, providing further evidence of a necessary steric blocking by TDP-43 for production of full-length STMN2 protein (Baughn et al., 2023).

1.3.2 *STMN2 knockout and lethality*

While the first group to genetically engineer a mouse *Stmn2* KO model discovered no effect on perinatal or embryonic lethality (Guerra San Juan et al., 2022), the research teams that followed found that *Stmn2*$^{-/-}$ mice exhibited reduced perinatal fitness after being born at expected Mendelian ratios (Krus et al., 2022; Li et al., 2023). Heterozygous mice genetically modified to contain the 2a cryptic exon, without the TDP-43 binding motif, developed normally despite a 50% reduction of full-length mouse *Stmn2* mRNA, while homozygous mutant mice had an 80% reduced survival in weaning, indicating developmental lethality due to a lack of *Stmn2* (Baughn et al., 2023). Further investigation revealed these variances between research groups may be a mouse strain-dependent phenotype, as one group found different survival rates between *Stmn2*$^{-/-}$ mice in C57BL/6J versus FVB:B6 mouse backgrounds (Lopez-Erauskin et al., 2023).

1.3.3 *Mouse models of STMN2*

Four stathmin-2 knockout mouse models have now been developed and characterized by the Eggan and Verhage (2022), DiAntonio and Milbrandt (2022), Chen and Huang (2023), and Lagier-Tourenne and Cleveland (2023) research groups, and the observed phenotypes are

consistent between models. A form of motor impairment, as assessed by rotarod, hanging wire test, or other basic measurement of motor function, was noted in all *Stmn2*$^{-/-}$ models, as was neuromuscular junction denervation and disorganization. Additionally, there is consensus pointing to a lack of compensation from the other Stathmin-family proteins (STMN1, STMN3, STMN4) in response to depletion or elimination of STMN2 (Guerra San Juan et al., 2022; Krus et al., 2022; Li et al., 2023; Lopez-Erauskin et al., 2023).

The Eggan and Verhage group discovered increased muscular atrophy in response to persistent NMJ denervation, and consequentially an increase in centralized nuclei in muscle cells. Disruption of microtubule dynamics including a decrease in neuronal β-III-Tubulin polymerization rate was found to be independent of total tubulin levels or free-to-polymerized tubulin ratios, indicating selective regulation of microtubule dynamics in the nervous system (Guerra San Juan et al., 2022). Other disruptions to microtubule dynamics, such as reduced polymerization rate (Krus et al., 2022), increased microtubule and neurofilament density (Lopez-Erauskin et al., 2023), and increased tubulin acetylation and decreased tubulin tyrosination resulting in increased microtubule stability but attenuated microtubule dynamics (Li et al., 2023), were observed when comparing *Stmn2*$^{-/-}$ mice to wild type counterparts.

Sensory issues were noted in *Stmn2*$^{-/-}$ mice along with reports of myelination, axon diameter, and axonal transport irregularities (Li et al., 2023). Other groups reported slower axonal conduction velocity and decreased tactile perception in *Stmn2*$^{-/-}$ mice (Lopez-Erauskin et al., 2023). Of note, an investigation into heterozygous *Stmn2*$^{+/-}$ mice revealed a slower and more progressive motor neuropathy along with sparing of the sensory pathway. These heterozygous

mice are claimed to be a better representation of the partial STMN2 protein loss found in ALS patients, and they do present NMJ denervation and functional deficits (Krus et al., 2022).

A rescue experiment involving the transgenic expression of human STMN2 in *Stmn2*$^{-/-}$ mice (h*STMN2*xm*Stmn2*$^{-/-}$) through a bacterial artificial chromosome (BAC) was sufficient to restore both motor function and NMJ innervation, paving the way for future therapeutics to target the stabilization and increased expression of stathmin-2 for ALS patients (Guerra San Juan et al., 2022).

1.3.4 *Zebrafish stmn2*

Zebrafish are an excellent vertebrate model to study disease as their organization of tissues and organs, including the brain and spinal cord, are largely conserved with other vertebrates. They regularly produce hundreds of externally fertilized embryos that are easy to manipulate genetically, they reach sexual maturity at 3 months of age, and they remain fertile for most of their lifespan. During larval stages of development, they are optically transparent, making them a powerful model for live-cell fluorescent imaging. Importantly, their genome also contains an ortholog for about 70% of human disease-causing genes, including the most significant genes in ALS pathophysiology (Howe et al., 2013; Kabashi et al., 2010).

Approximately 340 million years ago, zebrafish, along with other teleost, underwent a round of whole-genome duplication in a common ancestor. Stathmin-2 is thus represented by two genes, *stmn2a* and *stmn2b*, that both share 74% identity and 88% similarity with human *STMN2* and are 85% identical and 93% similar to each other (**Fig. 3**). As is the case in the mouse

genome, neither *stmn2a* nor *stmn2b* contain the 2a cryptic exon. At the time of this writing, no zebrafish stathmin-2 knockout models have been described. Here we present the development and preliminary characterization of the first *stmn2a* and *stmn2b* zebrafish knockout models.

Figure 3

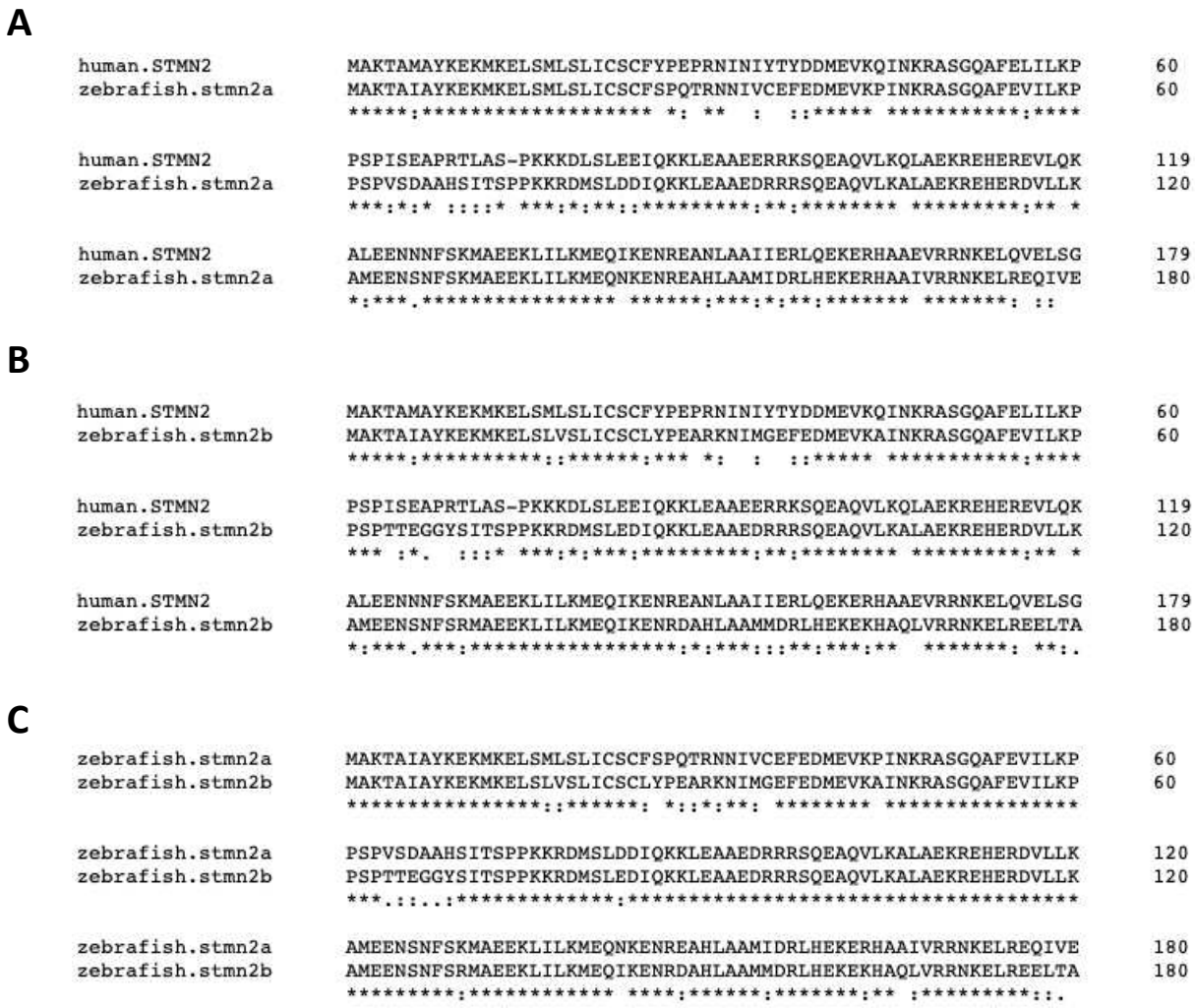

Figure 3 | Amino acid sequence comparison between **A**, human STMN2 and zebrafish Stmn2a, **B**, human STMN2 and zebrafish Stmn2b, and **C**, zebrafish Stmn2a and Stmn2b. Zebrafish Stmn2a and Stmn2b share 74% identity and 88% similarity with human STMN2 and are 85% identical and 93% similar to each other.

2. Materials and methods

Zebrafish housing and maintenance

Adult zebrafish (*Danio rerio*) of the Tübingen long fin (TL) and AB strains were maintained according to standard protocols (Westerfield, 1995) at 28.5°C under a 14/10 hour light/dark cycle in the animal research facility of the Montreal Neurological Institute (MNI), at McGill University (Montreal, Quebec, Canada). All experiments were approved by MNI's Animal Care Committee (ACC) and followed the guidelines from the Canadian Council for Animal Care (CCAC).

Cas9 mRNA and guide RNA synthesis

Synthesis of *Cas9* mRNA and guide RNA (gRNA) was performed using previously described methods (Jao et al., 2013; Vejnar et al., 2016). Target gRNA sites were identified using CRISPRscan (Moreno-Mateos et al., 2015), synthesized using the T7 MEGAscript kit (Invitrogen), and purified by phenol-chloroform extraction and ethanol precipitation. A zebrafish codon-optimized Cas9 (pT3TS-nCas9n, Addgene plasmid # 46757) was linearized with XbaI overnight and 1 μg of linear template DNA was used for *in vitro* transcription of mRNA using the T3 mMESSAGE mMACHINE® (Invitrogen) kit and purified by phenol-chloroform extraction and ethanol precipitation. The following gRNA target sites were used, with the protospacer-adjacent motif (PAM) site underlined:

5' GAAGAAGCTGGAGGCGGCTGAGG 3' for *stmn2a*, located in exon 3.

5' GAGGCACGCAAGAACATCATGGG 3' for *stmn2b*, located in exon 2.

CRISPR/Cas9 mutagenesis and screening for founder lines

Stmn2a KOs*, stmn2b* KOs*,* and double *stmn2a/b* KOs were generated using methods previously described by our laboratory (Armstrong et al., 2016). *Cas9* mRNA (100 ng/µL) and gRNA (100 ng/µL) were co-injected in ~2 nL volumes into zebrafish embryos at the one-to-two-cell stage of development. DNA cutting efficiency was evaluated through High Resolution Melting (HRM) analysis of 24 one-to-two-day post-fertilization (1-2 dpf) embryos per gRNA target (Erali & Wittwer, 2010). The most efficient gRNA target sites were selected for the creation of individual zebrafish lines with disruption of *stmn2a* and *stmn2b* reading frames and raised as F0s. Adult F0s were outcrossed with wild type zebrafish and fertilized embryos were screened for indel transmission using HRM.

HRM primer sequences for verification of *stmn2a* line:

Forward: 5’ GGCCCACAGCATCACCTCT 3’

Reverse: 5’ CATTTGTCTGTGTTTGCACTAACCC 3’

Primer sequences for verification of *stmn2b* line:

Forward: 5’ CGCAGCATACAAAGAGAAGATGAAGG 3’

Reverse: 5’ TCCTTCTCCACTGTGTCTCATTACTGG 3’

General screening and knockout generation

Adult zebrafish were individually separated and anesthetized with 1% tricaine (MS-222, Sigma) and a caudal fin clip was used to extract DNA. DNA was extracted (Extract-N-Amp™ Tissue PCR Kit, Millipore Sigma), and target sites were amplified by polymerase chain reaction (PCR) and followed by restriction fragment-length polymorphism (BbvCI and NlaIII for *stmn2a* and *stmn2b*, respectively, **Supplementary Fig. 1**). Sequencing (Genome Québec) was performed

on amplicons to identify the specific mutation of each founder line. Founder zebrafish carrying frameshift mutations resulting in premature stop codons were selected and homozygous carriers of each mutation were generated by in-crossing F1s to generate our *stmn2a* KO, *stmn2b* KO, and double *stmn2a/b* KO lines. Transgenic Tg[*Hb9:GFP*] fish, expressing GFP in their motor neurons, were crossed into the KO models to generate a double *stmn2a*$^{-/-}$*; stmn2b*$^{-/-}$*;* Tg[*Hb9:GFP*] line.

Primer sequences for verification of *stmn2a* line:

Forward: 5' TAAAAGGGCCTCAGGTCAGG 3'

Reverse: 5' GTTCTCAATGTGGCTGTCTTTTCC 3'

Primer sequences for verification of *stmn2b* line:

Forward: 5' GTACCCTCTGGCTTAAAACGTAGATG 3'

Reverse: 5' CCTCTCACTCATGAAACGAGCTTG 3'

In vitro **fertilization of zebrafish eggs**

The procedure was adapted and modified from the Draper and Moens group (Draper & Moens, 2009). Adult 6-month-to-1-year-old zebrafish were anesthetized using 0.04% MS-222 (Sigma-Aldrich) dissolved in system water. Females were blotted dry to prevent premature hydration and subsequent swelling of the extracted eggs and placed upside down on the middle crease of a plastic sheet (4 x 6 cm) folded in two. Eggs were squeezed out by applying pressure with the thumb on the area dorsal to the cloaca. Good quality eggs (yellow in color and dry) were collected with a spatula and placed in a 35 mm petri dish. Several females were pooled, if needed, to collect enough eggs for a successful fertilization. Males were blotted dry to prevent hydration and early activation of the sperm cells and placed upside down in a foam holder.

Sperm was extracted under the microscope by squeezing from the area anterior to the cloaca to the cloaca itself using a pair of fine tipped untextured forceps (Fisher Scientific). Good quality sperm (white and not watery) was collected using an aspirator equipped with a gel loading tip (0.6 mm O.D., Fisher Scientific) marked at every µL. Several males were pooled to get a minimum of 1 µL of sperm. Eggs were fertilized by adding the sperm and activating it with 300 µL of system water for 5 minutes at room temperature (23 °C). Then 4 mL of system water was added, and eggs were incubated for 3 hours at 28 °C. After this, fertilized eggs were transferred to 40 mL culture bottles and kept at 28 °C until needed for an experiment or for raising to maturity.

Larval motor function

Larval motor function was assessed using methods previously described by our laboratory (Armstrong & Drapeau, 2013). Individual larvae aged 52-54 hpf were placed in the center of an aquatic arena (150 mm petri dish) containing fresh system water, temperature controlled between 24 °C and 25 °C. Individual larvae were allowed to habituate to the environment for 30-60 seconds. A light touch to the tail of the larvae was applied using a pair of forceps, evoking a burst swimming motor response. Movement was recorded from above at 30 Hz (Grasshopper 2 camera, Point Gray Research) until the larvae either stopped moving or collided with the side of the arena. Total swim distance and mean swim velocities were quantified following manual movement tracking (Manual Tracking plugin, ImageJ).

RNA extraction and quantitative real time PCR (qRT-PCR)

RNA was extracted from 30 pooled 2 dpf larvae using the trizol-chloroform method. Purity and quality of RNA was verified using a NanoDrop® instrument. 2.5 µg of RNA was used to create a cDNA library using the SuperScript VILO cDNA Synthesis Kit (Invitrogen). Quantitative real-time PCR was performed on the cDNA libraries using the SYBR Green Supermix (Bio-Rad Laboratories). The delta-delta Ct method of relative quantification was performed with *gapdh* as an internal control (Livak & Schmittgen, 2001).

Primer sequences for RT-qPCR analysis of *stmn2a* line:

Forward: 5' GAACAAGGAAAACCGTGAGG 3'

Reverse: 5' CTTGTTCCTGCGGACGAT3'

Primer sequences for RT-qPCR analysis of *stmn2b* line:

Forward: 5' CTGAAAGCCATGGAGGAGAA 3'

Reverse: 5' ACCAGCTGAGCGTGCTTC 3'

Neuromuscular junction colocalization and axonal microtubule networks

Immunofluorescent microscopy experiments were performed to assess NMJ integrity. Double labelling of pre-synaptic and post-synaptic membranes was achieved usinga synaptotagmin 2 (Syt2, pre-synaptic) antibody and sulforhodamine-conjugated alpha-bungarotoxin markers (α-Btx, post-synaptic), as previously described (Armstrong & Drapeau, 2013). Briefly, 10 dechorionated 2 dpf zebrafish larvae were fixed in 4% paraformaldehyde (PFA) in phosphate-buffered saline solution (PBS) overnight at 4 °C with a gentle rotation. Larvae were then rinsed with PBS (3 x 15 minutes) and incubated with 1 mg/mL collagenase in PBS solution for 45 minutes at room temperature (RT). Larvae were again rinsed in PBS (3 x 15

minutes) and incubated in PBST (PBS, Triton X-100) for 30 minutes at RT and then incubated in a 10 mg/mL sulforhodamine-conjugated α-Btx in PBST solution for 30 minutes at RT. Following this, larvae were rinsed with PBST (3 x 15 minutes) and incubated for an hour in fresh blocking solution (2% Goat serum, 1% bovine serum albumin (BSA), 0.1% Triton X-100, 1% DMSO in PBS) at RT before being left overnight in block solution containing the Syt2 primary antibody (DSHB, 1:100). The next day larvae were rinsed with PBST (4 x 15 minutes) and incubated at RT for 5 hours in fresh blocking solution containing the secondary antibody (Alexa fluor 647, ThermoFisher, 1:1200). Larvae were rinsed with PBST (3 x 15 minutes) and incubated in PBST overnight at 4 °C with a gentle rotation and then placed in a solution containing 70% glycerol and mounted on glass slides for imaging. NMJs were visualized with a 60x/1.42 oil immersion objective on a Quorum Technologies microscope with a 89 NORTH LDI spinning disk confocal mounted on an Olympus BX61W1 fluorescence
Microscope, connected to a photometrics prime BSI camera. Images were acquired using Volocity software (Improvision).

Axon cutting and recovery

Wild type and double *stmn2a*$^{-/-}$; *stmn2b*$^{-/-}$ larvae were screened for the Tg[*Hb9:GFP*] transgene at 2 dpf. Individual fish expressing green fluorescence protein were selected for axon ablation. Selected larvae were embedded in 1% low melting point agarose, prepared with system water as solvent, at either 3 or 4 dpf. Pre-transection images of fluorescent ventral root projections were collected. A microinjection needle was then used to transect an individual ventral root axonal projection in the area near the cloaca. Cut ventral roots were imaged immediately after the transection, followed by a 24-hour image collection at various timepoints

on a 60x/1.42 water immersion objective on the same microscope described in the prior sub-section. Images were captured using the Velocity software. Complete ventral root projection degeneration was noted at the timepoint of either **a.** axonal regeneration begins OR **b.** all axonal fragments distal to the transection site have been degraded. Ventral root projection regeneration was noted to begin when a new growth cone sprouted from the proximal side of the transection site and was noted to be completed when the projection reaches >90% of the length of the initial ventral root.

Statistical analyses

All statistical analyses were performed using Prism 9 (GraphPad Software Inc.). Shapiro-Wilks test was used to test for normal sample distributions. Tests with only two samples were compared using unpaired students' t-tests. Kruskal-Wallis tests were used to compare data sets containing more than two non-normally distributed samples, followed by Dunn's post-hoc multiple comparisons test. One-way ANOVA followed by Tuckey's multiple comparisons test were used for normally distributed data sets containing more than two samples. Chi-squared tests were used to compare genotypic frequencies. Significance was assessed at $p < 0.05$.

3. Results

Generation of a *stmn2a*$^{-/-}$, a *stmn2b*$^{-/-}$, a double *stmn2a*$^{-/-}$; *stmn2b*$^{-/-}$, and of a double *stmn2a*$^{-/-}$; *stmn2b*$^{-/-}$; Tg[*Hb9:GFP*] zebrafish line

Previous studies investigating the role of Stathmin-2 in the context of ALS rely on cell or mouse KO models of Stathmin-2 (Guerra San Juan et al., 2022; Klim et al., 2019; Krus et al., 2022; Lopez-Erauskin et al., 2023; Melamed et al., 2019). Here we describe the first zebrafish KO model of Stathmin-2, represented by the *stmn2a* and *stmn2b* genes.

In zebrafish, both Stmn2a and Stmn2b are encoded by genes containing 5 exons (**Fig. 4A**). Multiple guide RNAs targeting the coding regions within exons 2 and 3 for each gene were tested. HRM analysis of F1 offspring revealed gRNA #6, targeting exon 3 of *stmn2a,* and gRNA #11, targeting exon 2 of *stmn2b,* were cutting DNA with the highest efficiency. Genetic sequencing revealed an 11-nucleotide deletion was generated in exon 3 of *stmn2a* and a 13-nucleotide deletion was generated in exon 2 of *stmn2b*, both of which produced premature stop codons in the *stmn2* transcript (**Fig. 4B**). Indels were transmitted to the next generation and could be identified through restriction fragment-length polymorphism, as BbvCI and NlaIII restriction sites were lost with the deletions in *stmn2a* and *stmn2b*, respectively. A double *stmn2a* and *stmn2b* KO was generated after multiple generations of breeding.

Our laboratory houses a transgenic Tg[*Hb9:GFP*] zebrafish line that expresses membrane-associated (farnesylated) green fluorescent protein (mGFP) in zebrafish motor neurons. *Stmn2a*$^{-/-}$ and *stmn2b*$^{-/-}$ lines were bred into our transgenic Tg[*Hb9:GFP*] line until a

stmn2a$^{-/-}$; *stmn2b*$^{-/-}$; Tg[*Hb9:GFP*] line was generated, offering the ability to investigate motor neuron development and regeneration in a live Stathmin-2 KO model.

We confirmed our mutations result in disrupted gene function through quantification of RT-qPCR expression patterns in 2 dpf larvae, corrected for *gapdh* expression, and discovered significantly reduced expression of *stmn2a* and *stmn2b* in homozygous mutant carriers for each gene, respectively. This suggests that the mutant transcripts are degraded through nonsense-mediated decay (**Fig. 4C**). Statistical analysis was done by the Mann-Whitney test, with significance assessed at $p < 0.05$.

Loss of *stmn2b* does not require compensation from *stmn2a*, but *stmn2a* loss may require compensation from *stmn2b*

In situ hybridization experiments and preliminary single-cell RNA-Seq data revealed higher *stmn2a* expression than *stmn2b* at most timepoints of early zebrafish development (Burzynski et al., 2009; Sur et al., 2023). Analysis of RT-qPCR expression patterns in 2 dpf larvae, corrected for *gapdh* expression, revealed a lack of compensation from *stmn2a* in *stmn2b*$^{-/-}$ zebrafish. In *stmn2a*$^{-/-}$ larvae, a trend towards compensation and increased expression from *stmn2b* was noted (**Fig. 4C**).

Figure 4

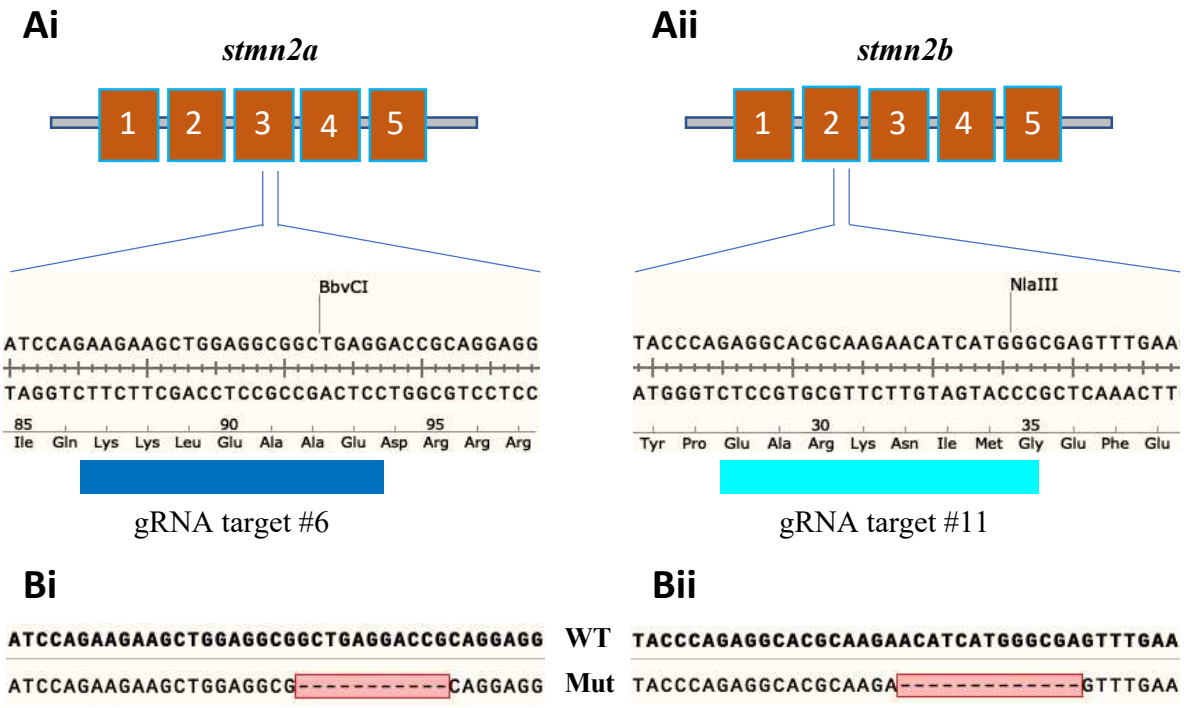
Ai
stmn2a
1 2 3 4 5
BbvCI
ATCCAGAAGAAGCTGGAGGCGGCTGAGGACCGCAGGAGG
TAGGTCTTCTTCGACCTCCGCCGACTCCTGGCGTCCTCC
85 90 95
Ile Gln Lys Lys Leu Glu Ala Ala Glu Asp Arg Arg Arg
gRNA target #6
Aii
stmn2b
1 2 3 4 5
NlaIII
TACCCAGAGGCACGCAAGAACATCATGGGCGAGTTTGAA
ATGGGTCTCCGTGCGTTCTTGTAGTACCCGCTCAAACTT
30 35
Tyr Pro Glu Ala Arg Lys Asn Ile Met Gly Glu Phe Glu
gRNA target #11

Bi
ATCCAGAAGAAGCTGGAGGCGGCTGAGGACCGCAGGAGG
ATCCAGAAGAAGCTGGAGGCG----------CAGGAGG
WT
Mut
Bii
TACCCAGAGGCACGCAAGAACATCATGGGCGAGTTTGAA
TACCCAGAGGCACGCAAGA----------GTTTGAA

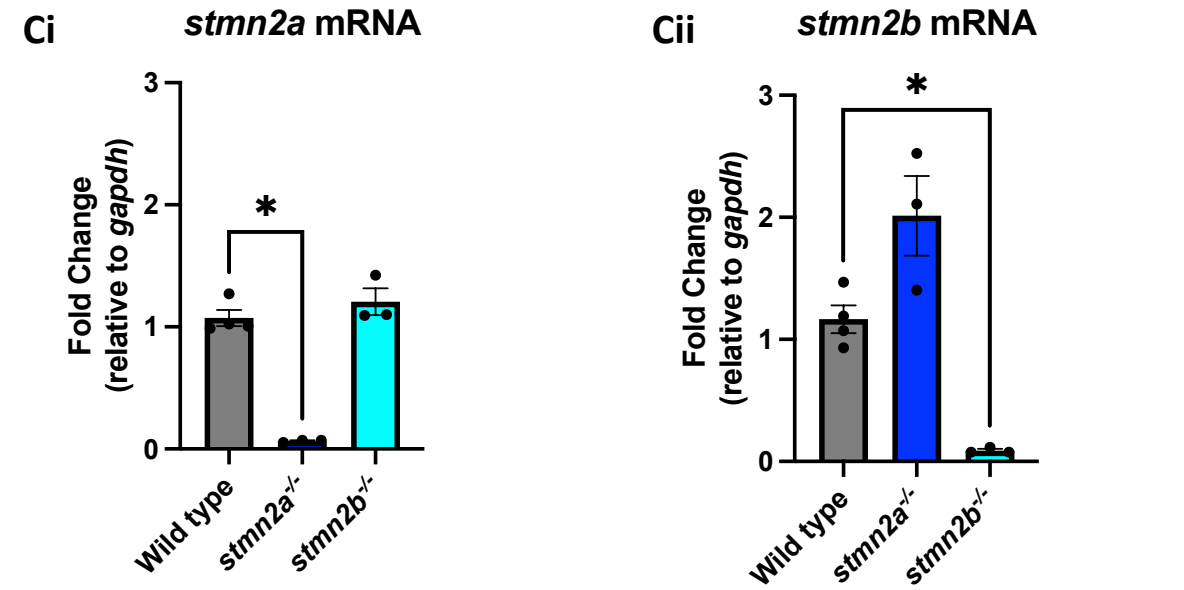
Ci
stmn2a mRNA
Fold Change (relative to gapdh)
0 1 2 3
*
Wild type
stmn2a-/-
stmn2b-/-
Cii
stmn2b mRNA
Fold Change (relative to gapdh)
0 1 2 3
*
Wild type
stmn2a-/-
stmn2b-/-

Figure 4 | Generation and RT-qPCR analysis of *stmn2a* and *stmn2b* KO zebrafish lines. Schematic representation of the 5 exons in *stmn2a* (**Ai**), and *stmn2b* (**Aii**). In **Ai**, gRNA target #6 in dark blue, located in exon 3, and a BbvCI restriction enzyme digestion site. In **Aii**, gRNA target #11 in light blue, located in exon 2, and an NlaIII restriction enzyme digestion site. These gRNAs were co-injected with *Cas9* protein leading to the creation of an 11-nucleotide deletion in exon 3 of *stmn2a* (**Bi**), leading to elimination of the BbvCI restriction site and generation of downstream premature stop codons. A 13-nucleotide deletion in exon 2 of *stmn2b* was created (**Bii**), leading to loss of the NlaIII restriction site and generation of downstream premature stop codons. **Ci** and **Cii**, qRT-PCR analysis of *stmn2* expression of 30 pooled 2 dpf larvae, relative to *gapdh* expression. As expected, a significant reduction in *stmn2a* expression in *stmn2a*$^{-/-}$ larvae, and a significant reduction in *stmn2b* in *stmn2b*$^{-/-}$ larvae was noted, confirming the mutant transcripts are targeted for nonsense-mediated decay. No *stmn2a* compensation was observed in the *stmn2b*$^{-/-}$ larvae, whereas a trend towards *stmn2b* compensation in *stmn2a*$^{-/-}$ larvae was noted. Statistical analysis by Mann-Whitney test, significance determined at $p < 0.05$. Sample sizes; wild type, N = 4 batches of 30 pooled larvae; *stmn2a*$^{-/-}$, N = 3; *stmn2b*$^{-/-}$, N = 3.

Double *stmn2a*$^{-/-}$; *stmn2b*$^{-/-}$ zebrafish display reduced survival despite no obvious morphological differences at larval stages of development

Mouse models of Stathmin-2 KO have shown variability in perinatal fitness depending on the mouse strain used, with some groups claiming increased perinatal lethality while others have found normal mendelian ratios surviving to adulthood (Guerra San Juan et al., 2022; Krus et al., 2022; Lopez-Erauskin et al., 2023). We sought to investigate survival fitness in our zebrafish Stathmin-2 KO model. While a Kaplan-Meier survival curve could not be generated due to a lack of full clutches of double *stmn2a*$^{-/-}$; *stmn2b*$^{-/-}$ fish, we turned to analyzing genetic frequencies from 295 screened adult zebrafish. All screened fish originated from either a *stmn2a*$^{+/-}$; *stmn2b*$^{+/-}$ X *stmn2a*$^{+/-}$; *stmn2b*$^{+/-}$ cross, or from a *stmn2a*$^{+/-}$; *stmn2b*$^{+/-}$ X *stmn2a*$^{-/-}$; *stmn2b*$^{+/-}$ cross. Assuming clutches of offspring respect normal mendelian ratios, a significant decrease in the number of double *stmn2a*$^{-/-}$; *stmn2b*$^{-/-}$ zebrafish was identified when compared to the expected count, indicating decreased survival in double *stmn2a*$^{-/-}$; *stmn2b*$^{-/-}$ zebrafish. Statistical significance assessed using a chi-squared test (**Fig. 5A, B**). Individual genotype frequencies can be seen in **Supplementary Fig. 2**.

At 2 dpf, no obvious morphological differences are apparent between wild type and double *stmn2a*$^{-/-}$; *stmn2b*$^{-/-}$ zebrafish, though a larger sample size will be necessary to note any differences in total size of the larvae (**Fig. 5C**). As such, we are uncertain of the mechanism that results in fewer double *stmn2a*$^{-/-}$; *stmn2b*$^{-/-}$ zebrafish reaching adulthood when compared to expected ratios.

Figure 5

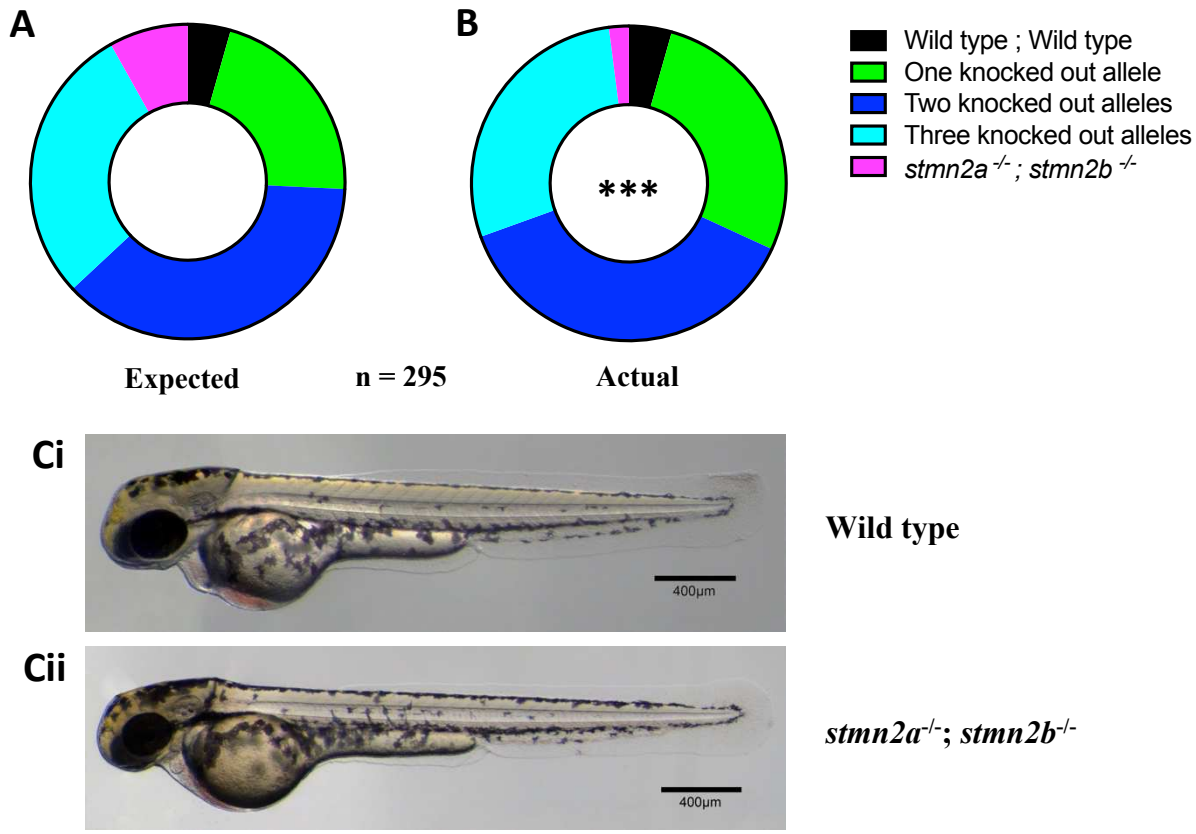

Figure 5 | Genotypic frequencies of adult zebrafish and larval morphology comparison. **A, B**, Genotypic frequencies of 295 adult zebrafish originating from *stmn2a*$^{+/-}$; *stmn2b*$^{+/-}$ X *stmn2a*$^{+/-}$; *stmn2b*$^{+/-}$ crosses, or from *stmn2a*$^{+/-}$; *stmn2b*$^{+/-}$ X *stmn2a*$^{-/-}$; *stmn2b*$^{+/-}$ crosses. **A**, expected genotypic frequencies and **B**, actual genetic frequencies. One knocked out allele refers to fish with either *stmn2a*$^{+/-}$; *stmn2b*$^{+/+}$ or *stmn2a*$^{+/+}$; *stmn2b*$^{+/-}$ genotypes. Two knocked out alleles refer to fish with *stmn2a*$^{+/-}$; *stmn2b*$^{+/-}$ or *stmn2a*$^{-/-}$; *stmn2b*$^{+/+}$ or *stmn2a*$^{+/+}$; *stmn2b*$^{-/-}$ genotypes. Three knocked out alleles refers to fish with *stmn2a*$^{-/-}$; *stmn2b*$^{+/-}$ or *stmn2a*$^{+/-}$; *stmn2b*$^{-/-}$ genotypes. Significance determined by Chi-squared test, $p < 0.001$. Individual genotype frequencies can be seen in **Supplementary Fig. 2**. **C**, example images of 2 dpf larvae for **Ci**, wild type and **Cii**, double *stmn2a*$^{-/-}$; *stmn2b*$^{-/-}$ larvae.

By 6 months of age, double *stmn2a*$^{-/-}$ & *stmn2b*$^{-/-}$ zebrafish present abnormal spinal curvature that does not affect survival, but may affect breeding

In wild type zebrafish, spinal curvature is a phenotype that will occasionally occur in older (>18 months old) fish, and very rarely earlier than that (Seda et al., 2023). In our double *stmn2a*$^{-/-}$; *stmn2b*$^{-/-}$ zebrafish, abnormal spinal curvature was noted in two of seven females, and seven out of ten males, by only 6 months of age. Age-matched wild type controls did not present with any spinal curvature of note (**Fig. 6**). Despite this, none of the 17 identified double *stmn2a*$^{-/-}$; *stmn2b*$^{-/-}$ zebrafish have died prematurely, indicating normal survival fitness once these mutants achieve adulthood.

Of the ten adult male double *stmn2a*$^{-/-}$; *stmn2b*$^{-/-}$ fish that have been identified, none of them have been capable of flushing eggs out of a female, regardless of the genotype of the female used. Motor function in adults has yet to be assessed, via free swim or swim tunnel experiments, but anecdotal data based on breeding patterns indicate the males may be too weak to effectively flush eggs out of a female during the breeding process. We have confirmed their sperm to be fertile, as *in vitro* fertilization experiments have been successful with the use of double *stmn2a*$^{-/-}$; *stmn2b*$^{-/-}$ sperm. Males expressing at least one copy of either *stmn2a* or *stmn2b* have been capable of flushing and fertilizing eggs from a female, including double *stmn2a*$^{-/-}$; *stmn2b*$^{-/-}$ females.

Figure 6

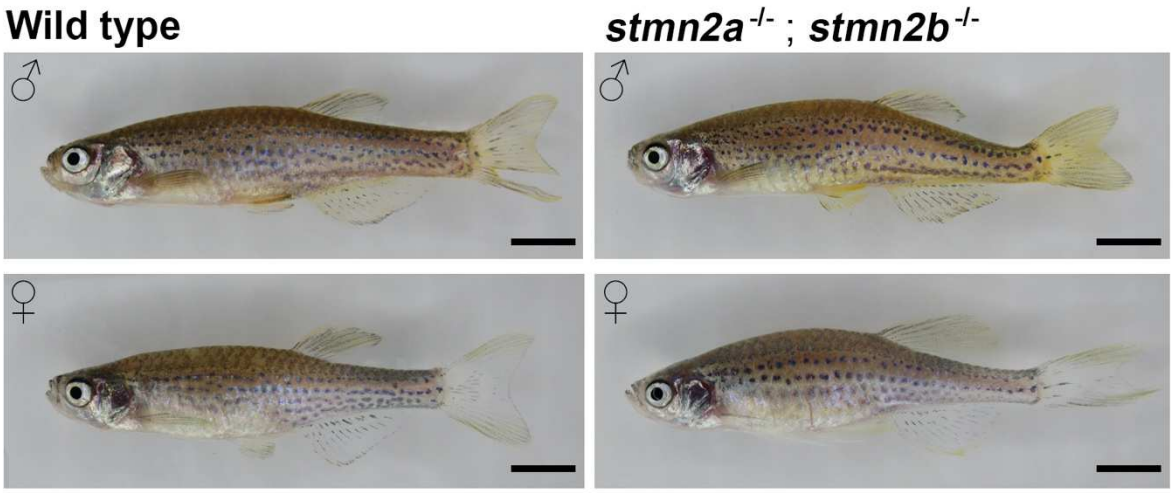

Figure 6 | Adult morphology comparison and *stmn2* KO spinal curvature.

Example images of six-month-old wild type (left) and double *stmn2a*$^{-/-}$; *stmn2b*$^{-/-}$ (right) zebrafish. Males in the top row, females in the bottom row. Spinal curvature is a rare phenotype that is rarely seen before 18 months of age. Age-matched wild type controls do not present any spinal curvature, whereas 6-month-old double *stmn2a*$^{-/-}$; *stmn2b*$^{-/-}$ fish present this phenotype in two of seven females and seven out of ten males.

Stmn2 KO zebrafish display a significant reduction in larval motor function

Motor function was assessed at 2 dpf by quantifying touch-evoked motor responses. This motor function assay revealed a significant reduction in total swim distance in *stmn2a*$^{-/-}$ and double *stmn2a*$^{-/-}$; *stmn2b*$^{-/-}$ larvae, while the *stmn2b*$^{-/-}$ larvae swam a similar total distance when compared to wild type larvae. Mean swim velocity was significantly reduced in *stmn2a*$^{-/-}$, *stmn2b*$^{-/-}$, and double *stmn2a*$^{-/-}$; *stmn2b*$^{-/-}$ larvae when compared to our measures of wild type mean swim velocity (**Fig. 7E**, **F**). Individual touch-response swim traces of the first 15 larvae assessed for each genotype are presented and indicate a distinct difference in motor function between wild type and *stmn2* KO larvae (**Fig. 7A**, **B**, **C**, **D**).

Figure 7

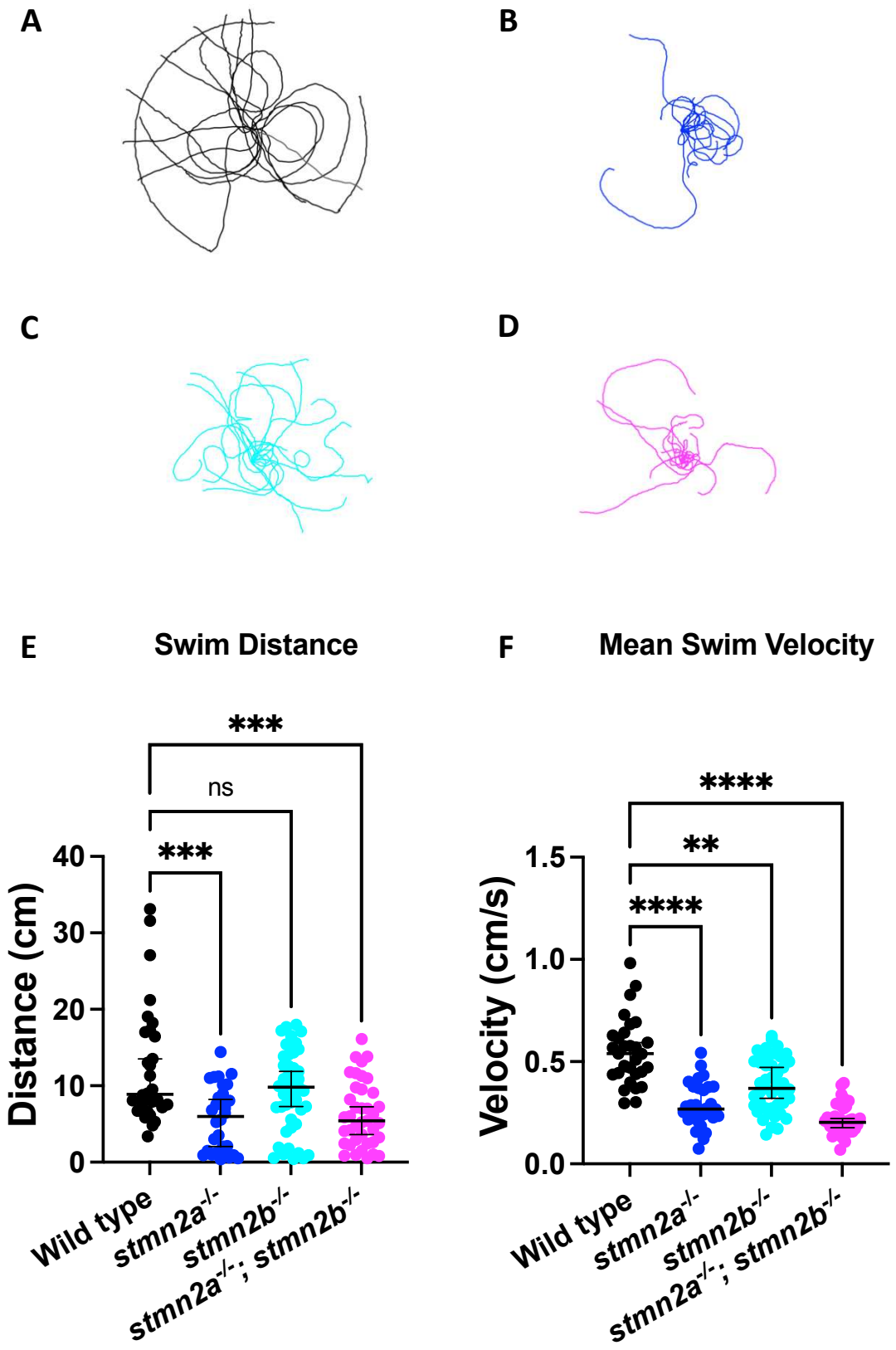
A
B
C
D
E
Swim Distance
F
Mean Swim Velocity
***
ns
***
Distance (cm)
40
30
20
10
0
Wild type
stmn2a-/-
stmn2b-/-
stmn2a-/-; stmn2b-/-
****
**
****
Velocity (cm/s)
1.5
1.0
0.5
0.0
Wild type
stmn2a-/-
stmn2b-/-
stmn2a-/-; stmn2b-/-

Figure 7 | 2 dpf touch-evoked motor response assay for *stmn2a*$^{-/-}$, *stmn2b*$^{-/-}$, and double *stmn2a* $^{-/-}$; *stmn2b*$^{-/-}$ larvae. Aquatic arena size of 150 mm was used and water temperature was maintained between 24 and 25 °C. Individual larvae were given 30-60 seconds to habituate to the environment before touch-evoked motor responses were assessed.

A, **B**, **C**, **D**, fifteen representative traces of touch-evoked motor responses in 2 dpf larvae, superimposed. **A**, wild type, **B**, *stmn2a*$^{-/-}$, **C**, *stmn2b*$^{-/-}$, and **D**, double *stmn2a*$^{-/-}$; *stmn2b*$^{-/-}$.

E, total swim distance measurement. *Stmn2a*$^{-/-}$ and double *stmn2a*$^{-/-}$; *stmn2b*$^{-/-}$ larvae displayed significantly reduced total swim distances while *stmn2b*$^{-/-}$ larvae performed similarly to wild type animals (Kruskal-Wallis multiple comparisons test, significance determined at $p < 0.05$). Mean swim distances and sample sizes; wild type (mean = 12.4 cm, n = 30), *stmn2a*$^{-/-}$ (mean = 5.7 cm, n = 30), *stmn2b*$^{-/-}$ (mean = 9.3 cm, n = 45), double *stmn2a*$^{-/-}$; *stmn2b*$^{-/-}$ (mean = 6.3, n = 39). **B**, mean swim velocity for 2 dpf larvae following a light tail touch. *stmn2a*$^{-/-}$, *stmn2b*$^{-/-}$, and double *stmn2a*$^{-/-}$; *stmn2b*$^{-/-}$ larvae all displayed significantly reduced mean swim velocities compared to wild type animals (Kruskal-Wallis multiple comparisons test, significance determined at $p < 0.05$). Average mean swim velocities and sample sizes; wild type (mean = 0.55 cm/s, n = 30), *stmn2a*$^{-/-}$ (mean = 0.9 cm/s, n = 30), *stmn2b*$^{-/-}$ (mean = 0.39 cm/s, n = 45), double *stmn2a*$^{-/-}$; *stmn2b*$^{-/-}$ (mean = 0.22 cm/s, n = 39).

Double *stmn2a*$^{-/-}$; *stmn2b*$^{-/-}$ zebrafish present decreased colocalization of pre- and post-synaptic markers

Reduced neuromuscular junction (NMJ) integrity has been described in previous ALS-mutant zebrafish models, where receptors were considered 'orphaned' when a pre-synaptic or post-synaptic puncta, within the area of ventral root branching, presented without colocalization (Armstrong & Drapeau, 2013; Bose et al., 2019). Immunofluorescence microscopy of ventral root projections of fixed 2 dpf larvae revealed a significant increase in orphaned pre-synaptic (syt2) puncta in *stmn2a*$^{-/-}$ as well as double *stmn2a*$^{-/-}$; *stmn2b*$^{-/-}$ zebrafish, whereas only double *stmn2a*$^{-/-}$; *stmn2b*$^{-/-}$ fish presented with a significant increase in orphaned post-synaptic puncta (αBtx) (**Fig. 8**). *Stmn2b*$^{-/-}$ animals presented comparable NMJ innervation to wild type animals. Example image of NMJ colocalization for all genotypes is available in **Supplementary Fig. 3**.

Figure 8

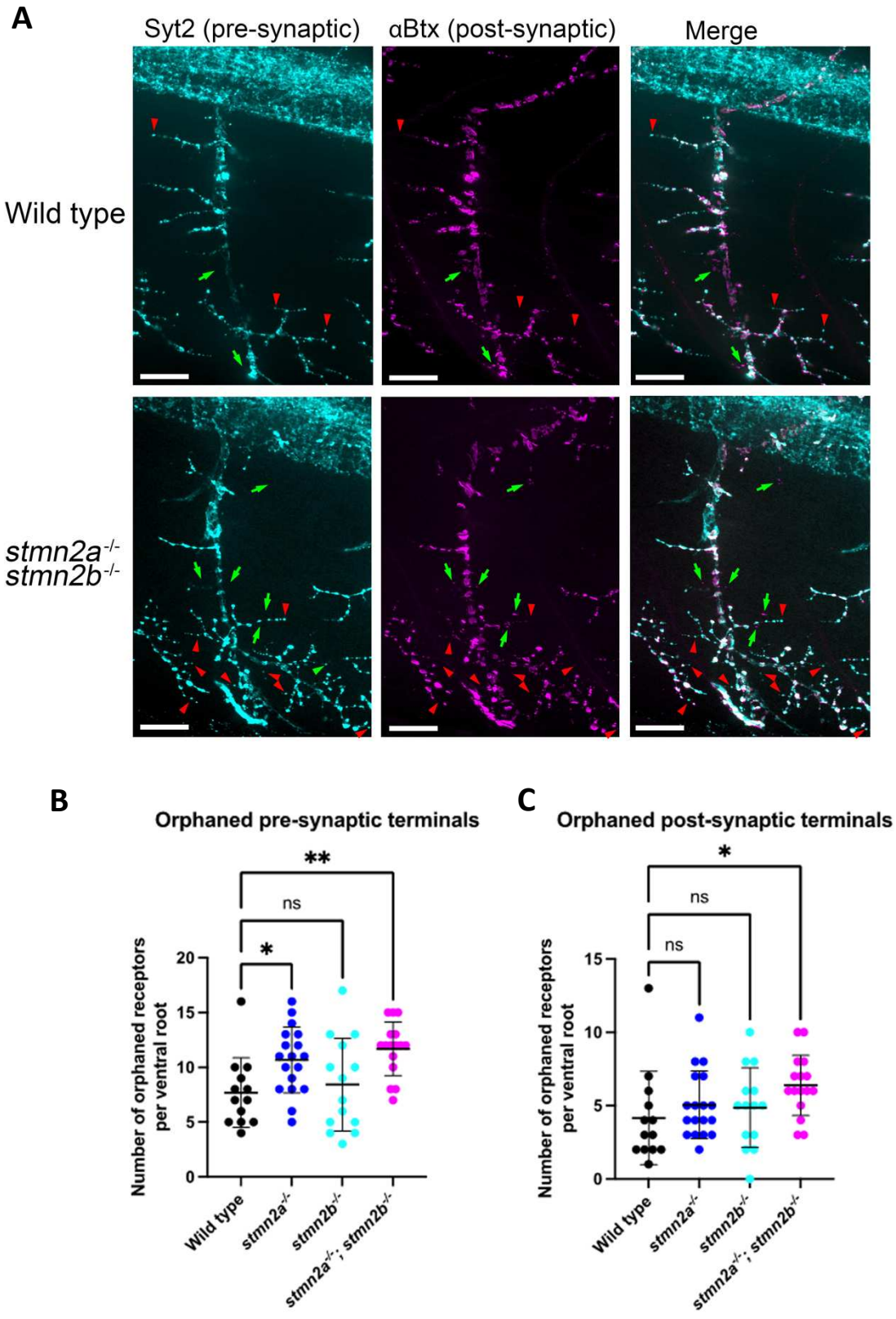
A
Syt2 (pre-synaptic)
αBtx (post-synaptic)
Merge
Wild type
stmn2a-/-
stmn2b-/-
B
Orphaned pre-synaptic terminals
Number of orphaned receptors per ventral root
**
ns
*
Wild type
stmn2a-/-
stmn2b-/-
stmn2a-/-; stmn2b-/-
C
Orphaned post-synaptic terminals
Number of orphaned receptors per ventral root
*
ns
ns
Wild type
stmn2a-/-
stmn2b-/-
stmn2a-/-; stmn2b-/-

Figure 8 | Neuromuscular junction abnormalities. **A**, example image of a 2 dpf wild type (top) and a double *stmn2a*$^{-/-}$; *stmn2b*$^{-/-}$ (bottom) trunk ventral root projection branching. Syt2 (pre-synaptic marker) in cyan, αBtx (post-synaptic marker) in magenta. Red arrows indicate orphaned pre-synaptic terminals, green arrows indicate orphaned post-synaptic terminals. **B,** quantification of orphaned pre-synaptic terminals and **C**, quantification of orphaned post-synaptic terminals. *stmn2a*$^{-/-}$ and double *stmn2a*$^{-/-}$; *stmn2b*$^{-/-}$ larvae present a significant increase in orphaned pre-synaptic terminals while only double *stmn2a*$^{-/-}$; *stmn2b*$^{-/-}$ larvae present an increase in orphaned post-synaptic terminals. Statistical analysis by Kruskal-Wallis test followed by Dunn's multiple comparisons. Significance was assessed at $p < 0.05$.

Double *stmn2a*$^{-/-}$; *stmn2b*$^{-/-}$ zebrafish may display impaired regeneration following ventral root nerve injury

This project is ongoing, and all preliminary results presented in this sub-section are anecdotal. A 3 dpf wild type; Tg[*Hb9:GFP*] larva was embedded in low melting point agarose and a single ventral root projection was transected with a microinjection needle (**Fig. 9A**). Within ~8 hours, the axon had fully degenerated, and within 24 hours, a new axon had replaced the transected one (**Fig. 9B**). We next tested the same experimental procedure on a 3 dpf *stmn2a*$^{-/-}$*; stmn2b*$^{-/-}$*;* Tg[*Hb9:GFP*] larva (**Fig. 9C**) and discovered an increase in the length of time it took the axon to degenerate, around 12-14 hours. More importantly, no axonal regeneration was noted in the region of the originally transected ventral root stump; even after 24 hours, no growth cone was observed (**Fig. 9D**). The experiment was repeated with a 4 dpf *stmn2a*$^{-/-}$*; stmn2b*$^{-/-}$*;* Tg[*Hb9:GFP*] larva, and an axon degeneration time of ~12-14-hours was noted. As with the 3 dpf larva, no new growth cone was sprouted from the ventral root stump. This ventral root was imaged for 24 hours. All zebrafish larvae remained alive throughout the entire course of the experiment. Our preliminary findings suggest a significant role for Stmn2a/b in axon maintenance and regeneration in zebrafish larvae.

Figure 9

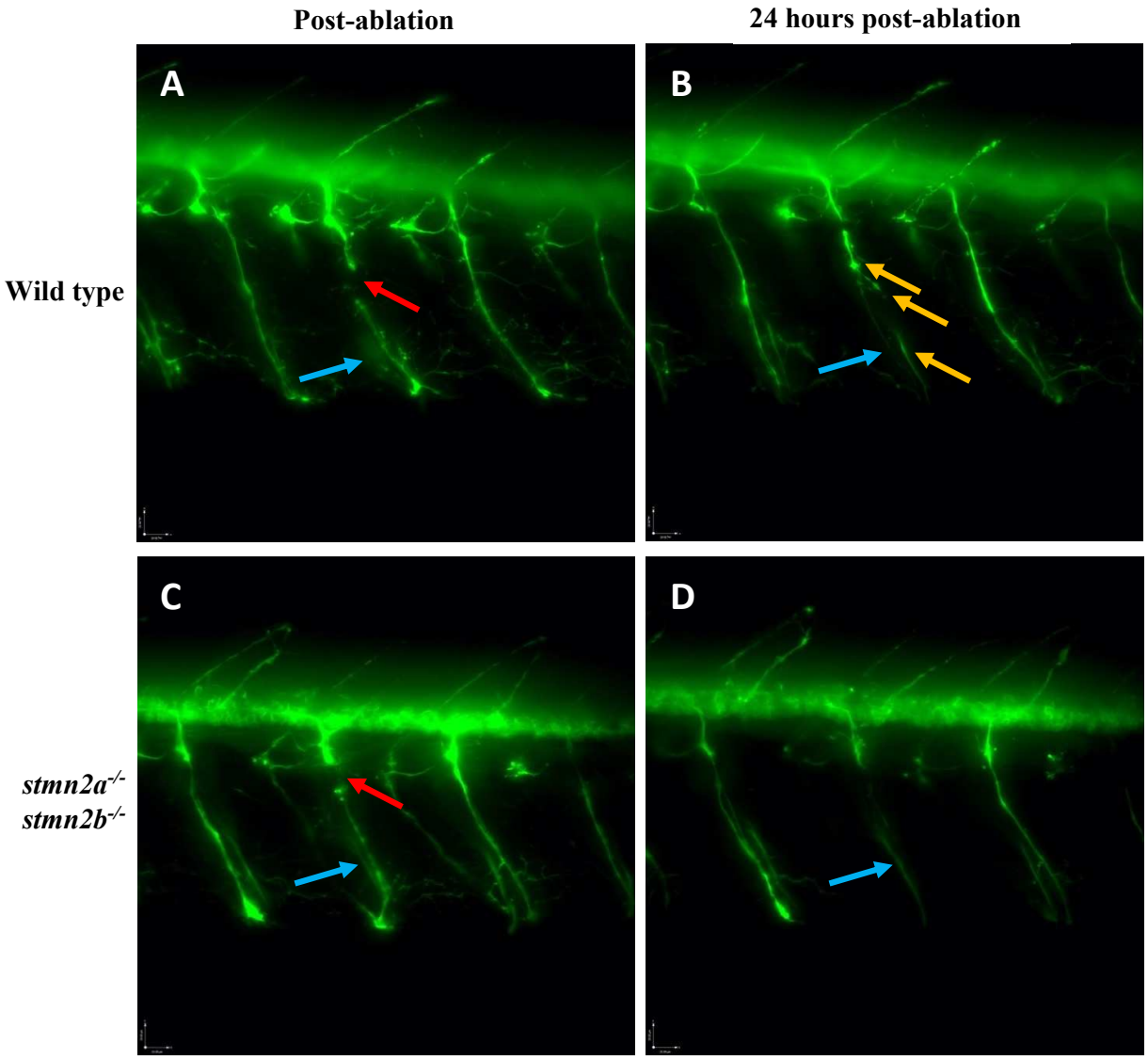

Figure 9 | Axon regeneration following injury at 3 dpf and regeneration at 4 dpf of (**A**, **B**) wild type; Tg[*Hb9:GFP*] and (**C**, **D**) double *stmn2a*$^{-/-}$*; stmn2b*$^{-/-}$*;* Tg[*Hb9:GFP*] zebrafish larvae. In red, location of microinjection needle transection of a single ventral root projection. In blue, the untouched ventral root on the other side of the fish. In orange, the regenerated axon in the wild type animal, 24 hours following injury. No regeneration is observed in the double *stmn2a*$^{-/-}$*; stmn2b*$^{-/-}$ fish.

4. Discussion and Conclusion

4.1 Discussion

ALS is a multifactorial disease that can differ significantly in clinical presentation between patients. However, some aspects of the disease remain predictable and expected for a significant majority of patients. Regardless of whether a patient's disease is of genetic origin (fALS, 10% of cases) or without a known genetic cause (sALS, 90% of cases), approximately 97% of all ALS patients present with some TDP-43 pathology (Neumann et al., 2006). TDP-43 has a significant role in RNA metabolism including the maintenance of RNA stability, transport, and splicing (Buratti & Baralle, 2001, 2008). These functions can become disrupted in ALS patients following the nuclear depletion and cytoplasmic mislocalization of the protein, resulting in downstream effects on multiple physiological pathways (Ling et al., 2013). Pharmacological targeting of TDP-43 is likely to be difficult due to its ubiquitous expression and complex network of connected protein pathways, leading to a strong risk of off-target side effects. Debate over whether TDP-43 pathology results in a loss-of-function disease mechanism, gain-of-toxic-function mechanism, or a combination of the two, adds an additional layer of difficulty when discussing therapeutic intervention targeting TDP-43 specifically (Lee et al., 2011). Instead, focus should be placed on downstream targets of TDP-43 that may be affected in ALS patients, with STMN2 being one of the more striking examples of misregulated transcripts observed in patients.

The discovery of a cryptic exon (exon 2a) in *STMN2*'s pre-mRNA that contains a cryptic 3' splice site, a premature stop codon, a premature polyadenylation site, and, most importantly, TDP-43 binding motifs, has been one of the latest and most significant discoveries in ALS-

related research in recent years (Baughn et al., 2023; Klim et al., 2019; Melamed et al., 2019). Nuclear depletion of TDP-43 in ALS patients exposes this cryptic exon to RNA processing factors that result in the production of a truncated and non-functional STMN2 protein, and testing of post-mortem ALS-patient spinal motor neurons has confirmed increased levels of this non-functional protein and decreased levels of full-length STMN2 (Klim et al., 2019; Melamed et al., 2019).

Animals, outside of primates, do not contain this cryptic exon in their respective *STMN2* ortholog. As a result, all models of *STMN2* KO, including murine and zebrafish models, offer the ability to study the effect of STMN2 depletion in a way that is isolated from TDP-43 regulation. While this can be seen as a limitation, as a major regulator of STMN2 expression is absent in these models, it is also a convenience, as it allows a more confined approach to the study of Stmn2. This is especially noteworthy given the recent work by the Cleveland group in confirming the cryptic splicing mechanism, as knocking in the cryptic exon into the mouse genome was sufficient to trigger regulation by TDP-43 (Baughn et al., 2023). There are currently no known mutations in *STMN2* that have been directly linked to ALS, despite a 2021 report claiming an increased risk of early-onset and rapidly progressing disease for those with ≥ 24 non-coding CA repeats between exons 3 and 4 (Theunissen et al., 2021). Further investigation has revealed this to not be associated with a higher risk of aggressive forms of ALS (Doronzio et al., 2023; Grima et al., 2022; Ross et al., 2022).

Mouse KO models of STMN2 have individually presented similar phenotypes, including but not limited to: general and progressive motor impairment, neuromuscular junction

fragmentation and denervation, and disrupted microtubule and tubulin networks (Guerra San Juan et al., 2022; Krus et al., 2022; Li et al., 2023; Lopez-Erauskin et al., 2023). No other animal STMN2 KO models have been described, a void this thesis project has addressed. Through CRISPR/Cas9 mutagenesis, our laboratory has developed the first zebrafish *stmn2* knockout model that includes an 11-nucleotide deletion in exon 3 of *stmn2a*, and a 13-nucleotide deletion in exon 2 of *stmn2b*, both of which produce premature stop codons that result in the mRNA transcripts being targeted for nonsense-mediated decay. Single-cell RNA-Seq data (Sur et al., 2023) and *in situ* hybridization experiments (Burzynski et al., 2009) suggest increased *stmn2a* expression relative to *stmn2b* in developing zebrafish. In agreement, we have found no compensation from *stmn2a* following *stmn2b* depletion, whereas a trend was discovered for *stmn2b* compensation for *stmn2a* loss. This suggests normal *stmn2a* expression, in the absence of *stmn2b*, is sufficient, while normal *stmn2b* expression, in the absence of *stmn2a,* is not. Finding an antibody that is specific for both *stmn2a* and *stmn2b* while not labeling the other members of the stathmin family of proteins has proven difficult in the zebrafish, so protein-level quantification will be necessary to confirm this finding. Based on the literature, no compensation from other stathmin-family proteins is expected, but that will need to be confirmed in the zebrafish.

In agreement with most mouse models of stathmin-2 knockout, we have found reduced survival in double *stmn2a*$^{-/-}$; *stmn2b*$^{-/-}$ zebrafish at developmental stages, as assessed by chi-squared test of genotypic frequencies. A Kaplan-Meier survival curve could not be generated due to a lack of full clutches of double *stmn2a*$^{-/-}$; *stmn2b*$^{-/-}$ zebrafish, though we anticipate being able to perform this experiment soon as more adult double KOs are identified which might be able to

produce viable clutches of fertilized eggs. Survival fitness appears normal at 3 months of age as none of the 17 identified double *stmn2a*$^{-/-}$; *stmn2b*$^{-/-}$ zebrafish have died prematurely, a similar pattern to what is seen in the mouse models. The mechanism behind this is still undetermined, though we suggest a cell division deficit during development may be caused by a disrupted microtubule network in stathmin-2 knockout models. Further investigation into this early survival defect is required to come to a more conclusive understanding of what is causing it.

In vitro fertilization using double *stmn2a*$^{-/-}$; *stmn2b*$^{-/-}$ sperm has confirmed the male gametes are able to fertilize eggs, however their consistent inability to breed naturally is noteworthy. Despite 20+ breeding attempts of double *stmn2a*$^{-/-}$; *stmn2b*$^{-/-}$ males with double *stmn2a*$^{-/-}$; *stmn2b*$^{-/-}$ females, none of them have resulted in fertilized eggs. One future series of experiments that are likely to be undertaken by the Armstrong lab will be to assess adult motor function using a free swim and modified sprint swim test using a swim tunnel (Gilbert et al., 2014), where a deficit in observed motor function could explain breeding problems for double *stmn2a*$^{-/-}$; *stmn2b*$^{-/-}$ fish. We have noted a trend towards increased spinal curvature in double *stmn2a*$^{-/-}$; *stmn2b*$^{-/-}$ fish at 6 months of age, an early presentation of what is normally a rare phenotype (Seda et al., 2023). An investigation into spinal curvature in zebrafish revealed that normal cilia biology, composed primarily of microtubule structures, is critical for spine maintenance (Boswell & Ciruna, 2017; Munoz-Montecinos et al., 2021). We suggest poor cilia dynamics, due to disrupted microtubule networks resulting from Stmn2 depletion, may be a factor contributing to this spinal curvature in our mutant model.

We have observed a larval motor phenotype in our *stmn2a*$^{-/-}$, *stmn2b*$^{-/-}$ and double *stmn2a*$^{-/-}$; *stmn2b*$^{-/-}$ zebrafish at 2 dpf, analogous to what is observed in mouse models. All three zebrafish models of *stmn2* KO present a significant reduction in touch-response assay mean swim velocity, and only *stmn2a*$^{-/-}$ and double *stmn2a*$^{-/-}$*; stmn2b*$^{-/-}$ larvae present a reduction in total swim distance. Similarly, double *stmn2a*$^{-/-}$*; stmn2b*$^{-/-}$ larvae present reduced pre- and post-synaptic neuromuscular junction colocalization, while *stmn2a*$^{-/-}$ larvae present an increase in orphaned pre-synaptic terminals exclusively. *Stmn2b*$^{-/-}$ larvae show normal innervation, albeit a trend towards reduced colocalization. We believe this NMJ denervation to be primarily responsible for the poor larval motor performance, though other factors may be at play. Muscle cell abnormalities that have been reported in mice (Guerra San Juan et al., 2022) may also be occurring in our zebrafish models. Additionally, it is possible that the touch response assay may be affected by sensory deficits, as it relies on first integrating tactile sensation and then driving activity in sensory neurons, both of which could be impaired in our Stmn2 KO model. None of the 2 dpf larvae failed to react to the tail touch, suggesting that at this stage in development the sensory system of the larvae is intact. As sensory defects have been reported in multiple Stmn2 KO models (Krus et al., 2022; Li et al., 2023; Lopez-Erauskin et al., 2023), however, we cannot fully discount it occurring in our model. One way to address this would be to carry out electrophysiological recordings, adult motor-function assays (free swim, sprint swim test), whole trunk cross-section muscle analysis, and spinal cord immunolabeling to help reveal the complete mechanism behind the motor deficits, including the observed mean swim velocity deficits in *stmn2b*$^{-/-}$ larvae that do not present with abnormal NMJs.

In contrast to a study in mouse dorsal root ganglion (DRG) cells that suggested faster axon degeneration time following *stmn2* depletion (Shin et al., 2012), we have anecdotally observed slower axon degeneration time in our double *stmn2a*$^{-/-}$; *stmn2b*$^{-/-}$; Tg[*Hb9:GFP*] zebrafish model when compared to wild type animals. This may be due to differences in axon degeneration properties between mouse cell cultures and zebrafish larvae, and we believe further data collection through this experiment will lead to a more conclusive understanding of Stmn2 involvement in axon repair following injury. Importantly, we also anecdotally observed a failure of axons to regenerate in our double *stmn2a*$^{-/-}$*; stmn2b*$^{-/-}$*;* Tg[*Hb9:GFP*] model (n = 2), whereas wild type Tg[*Hb9:GFP*] fish (n = 1) had nearly complete axon regeneration within 24 hours following transection. Future studies could continue this data collection as it would likely shed more light into Stmn2's role in axon protection and regeneration. This would aid in furthering our understanding of what could be occurring in human motor neurons and build upon what has been already described for human iPSCs models of TDP-43 and STMN2 (Klim et al., 2019; Melamed et al., 2019).

JNK1 is a kinase that can reduce STMN2 function and trigger degradation through phosphorylation of serine residues in STMN2's N-terminal domain. Inhibition of JNK1 is reported to provide axonal protection through attenuation of this downstream effect on stathmin-2 (Klim et al., 2019; Tararuk et al., 2006). The JNK1-targeted serine residues are conserved in the zebrafish genome, and we may consider experimenting with JNK1 inhibition in individual *stmn2a*$^{-/-}$ or *stmn2b*$^{-/-}$ fish as this may be more representative of STMN2 expression in ALS patients. It is worth mentioning that this mechanism could be worth exploring from a therapeutic perspective, as ALS patients do not present complete STMN2 depletion.

Once clutches of double *stmn2a*$^{-/-}$; *stmn2b*$^{-/-}$ zebrafish become available, a future series of experiments could attempt to rescue the observed motor and neuromuscular junction defect phenotypes through transgene expression of full-length or truncated human *STMN2*. We expect to see restoration of the ventral root's ability to regrow motor axons following expression of full length *STMN2.* That said, transgene expression of the suggested truncated form of *STMN2* observed in ALS would not confer the ability for ventral roots to regrow injured axons. To do this, a student would perform microinjections of *stmn2* constructs into developing blastocysts and investigate if motor function, neuromuscular junction colocalization, and ventral root regeneration is improved in our KO model. We hypothesize the results of this future experiment will match previously performed *in vitro* rescue experiments (Klim et al., 2019; Melamed et al., 2019). The ongoing phase 1 clinical trial by QurAlis (clinical trial number: NCT05633459) is evaluating the safety of an antisense oligonucleotide (ASO) targeting STMN2 mRNA, attempting to mimic TDP-43 binding and prevent the use of the cryptic 3' splice site. We believe this to be an appropriate target for patients with TDP-43 pathology and reduced levels of STMN2. It is also possible that the truncated form of STMN2 could be a potential biomarker for ALS, helping patients begin treatment sooner.

Our preliminary characterization of a zebrafish *stmn2* KO model has revealed similar phenotypes to what is observed in mouse *STMN2* KOs as well as ALS patients presenting TDP-43 pathology. We believe our zebrafish stathmin-2 KO model will be useful for future drug screening as this model offers a unique opportunity to evaluate water-soluble compounds directly in the fish's environment. Despite ALS showing the most significant disruption in genes involved in microtubule regulation among brain diseases, there are currently zero ongoing

clinical trials attempting to repurpose microtubule-stabilizing drugs for ALS treatment (Varidaki et al., 2018). It should be noted that a common side effect of this class of drugs is peripheral neuropathy, a symptom we would like to prevent in ALS patients.

We propose that our zebrafish *stmn2* KO model can be used for semi-high throughput testing of drugs targeting microtubule dynamics. Zebrafish are a well-established model for drug screening of water-soluble compounds, as zebrafish embryos can absorb small molecules at physiological drug concentrations directly from their environment (Patton et al., 2021). Motor and neuromuscular junction evaluations can be performed following developmental treatment with drugs targeting the microtubule network, many of which are already been approved by the Food and Drug Administration (FDA) and can potentially be repurposed for the treatment of ALS.

4.2 Conclusion

This thesis explores the development and initial characterization of a novel zebrafish *stmn2* knockout model. Stathmin-2 has recently emerged as a protein of relevance in ALS as most patients present significantly reduced levels of the full-length protein, resulting from misprocessing by loss of TDP-43. We utilized the CRISPR/Cas9 mutagenic system to produce frame-shift deletions in both copies of zebrafish *STMN2* (*stmn2a* and *stmn2b*), resulting in both transcripts being targeted for nonsense-mediated decay. An additional double *stmn2a*$^{-/-}$; *stmn2b*$^{-/-}$; Tg[*Hb9:GFP*] transgenic model was developed, allowing for the observation of individual ventral root projections through GFP expression in motor neurons. Using qRT-PCR approaches we observed that there was no compensation from *stmn2a* in response to *stmn2b* loss, but a trend towards compensation by *stmn2b* in *stmn2a*$^{-/-}$ animals was observed. Despite no gross morphological differences between *stmn2* KO and wild type fish at larval stages of development, reduced survival was noted in the former. By 6 months of age, a spinal curvature phenotype appears in approximately half of the *stmn2a/b* KOs, potentially contributing to their breeding difficulty. Double *stmn2a*$^{-/-}$; *stmn2b*$^{-/-}$ larvae present a significant motor function deficit as well as a decrease in colocalization of pre- and post-synaptic NMJ markers. Furthermore, *stmn2a*$^{-/-}$ larvae present a significant decline in motor function and an increase in orphaned pre-synaptic terminals, and *stmn2b*$^{-/-}$ larvae present a milder motor function deficit and have normal NMJ pre- and post-synaptic marker colocalization. Preliminary axon transection experiments suggest a slower axon degeneration time and complete elimination of axon regeneration in double *stmn2a*$^{-/-}$; *stmn2b*$^{-/-}$; Tg[*Hb9:GFP*] larvae. Overall, we postulate that our mutant models recapitulate certain key phenotypes of ALS patients presenting TDP-43 pathology and reduced STMN2 levels. The ALS patient population is in desperate need of new treatments, and we believe this

novel animal model will contribute significantly to the uncovering of ALS-related pathways that could be targeted for therapeutic development.

5. Supplementary Figures

Supplementary Figure 1

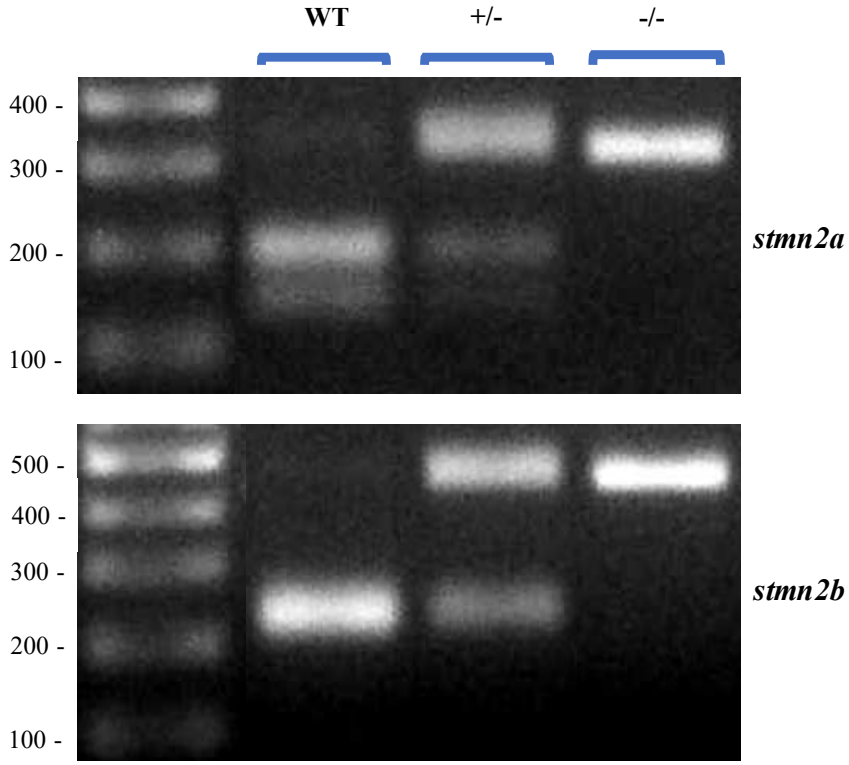

Supplementary Figure 1 | Restriction enzyme fragment-length polymorphism for *stmn2a* (top) and *stmn2b* (bottom). Wild type animals retain the BbvCI (*stmn2a*) and NlaIII (*stmn2b*) digestion sites, resulting in two small bands (left column, 138 and 188 bp for *stmn2a*; 216 and 239 bp for *stmn2b*). Heterozygous KO animals have one large uncut band (326 bp for *stmn2a*, 455 bp for *stmn2b*) and two small bands (middle column). Homozygous KO animals have complete elimination of the restriction enzyme digestion site, resulting in only one large uncut band (right column).

Supplementary Figure 2

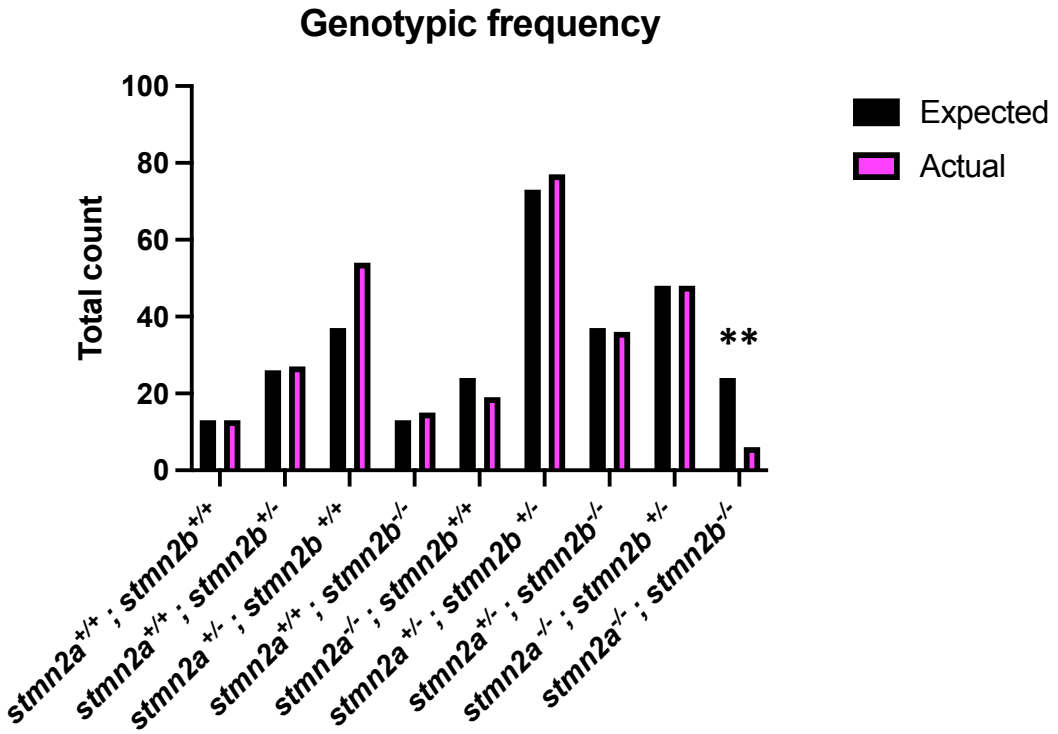

Supplementary Figure 2 | Expected (black) and actual (pink) observed genotypic ratios from 295 screened adult zebrafish from either a *stmn2a*$^{+/-}$; *stmn2b*$^{+/-}$ X *stmn2a*$^{+/-}$; *stmn2b*$^{+/-}$ cross, or from a *stmn2a*$^{+/-}$; *stmn2b*$^{+/-}$ X *stmn2a*$^{-/-}$; *stmn2b*$^{+/-}$ cross. A significant reduction of identified double *stmn2a*$^{-/-}$; *stmn2b*$^{-/-}$ fish was noted when compared to the expected frequency, as assessed by Chi-square test. Significance determined at $p < 0.05$.

Supplementary Figure 3

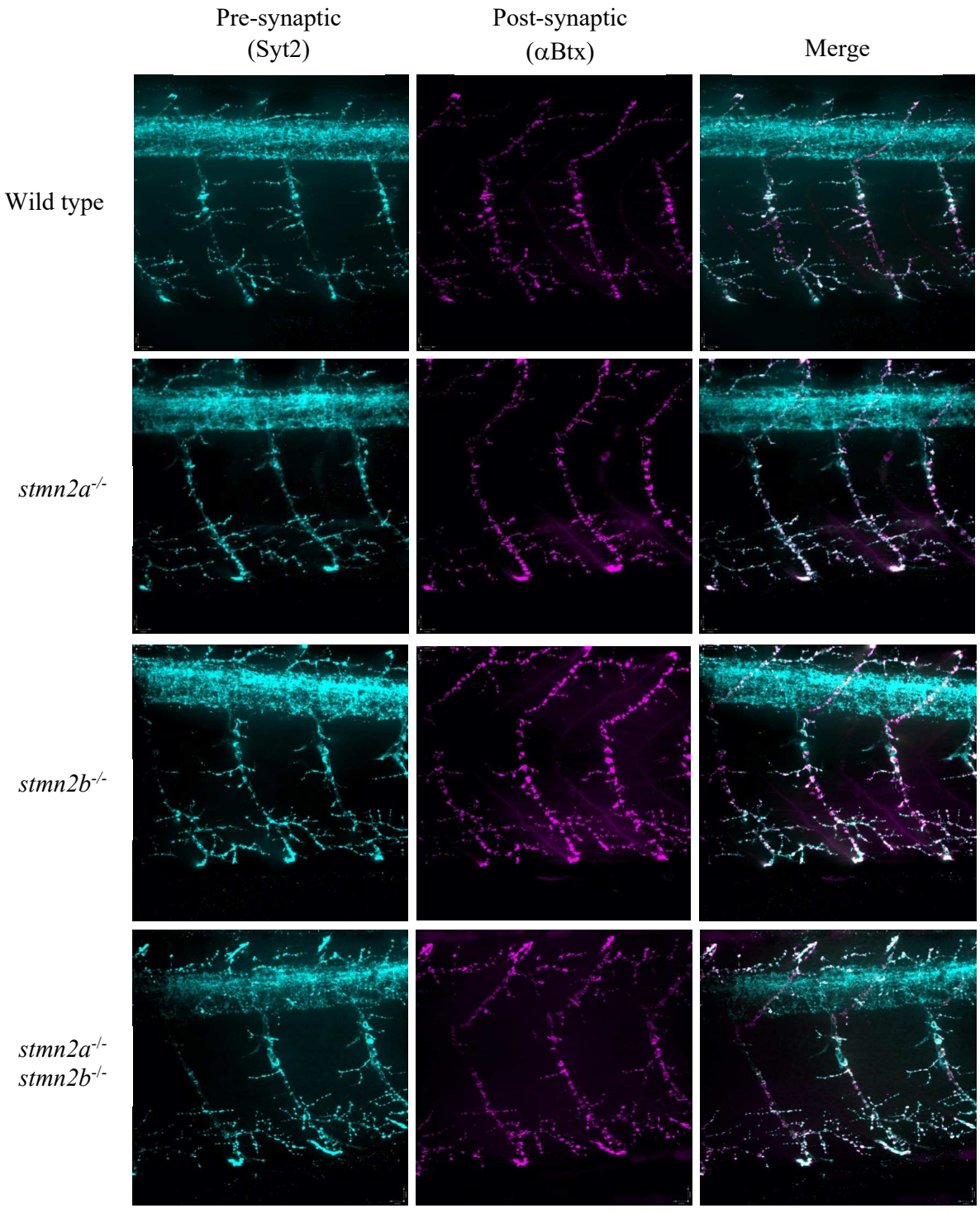

Supplementary Figure 3 | Example images of neuromuscular junction colocalization for wild type (top row), *stmn2a*$^{-/-}$ (second row), *stmn2b*$^{-/-}$ (third row), and double *stmn2a*$^{-/-}$; *stmn2b*$^{-/-}$ (bottom row) 2 dpf larvae. In cyan (left column), syt2-labeled pre-synaptic terminals, in magenta (middle column), αBtx-labeled post-synaptic terminals, and the merged images (right). Images were captured in the region near the cloaca using a 60x/1.42 oil immersion objective on a Quorum Technologies microscope with a 89 NORTH LDI spinning disk confocal mounted on an Olympus BX61W1 fluorescence microscope, connected to a photometrics prime BSI camera. Images captured using Velocity software

6. Bibliography

Al-Chalabi, A., & Hardiman, O. (2013). The epidemiology of ALS: a conspiracy of genes, environment and time. *Nat Rev Neurol*, *9*(11), 617-628. https://doi.org/10.1038/nrneurol.2013.203

Appel, S. H. (1981). A unifying hypothesis for the cause of amyotrophic lateral sclerosis, parkinsonism, and Alzheimer disease. *Ann Neurol*, *10*(6), 499-505. https://doi.org/10.1002/ana.410100602

Arai, T., Hasegawa, M., Akiyama, H., Ikeda, K., Nonaka, T., Mori, H., Mann, D., Tsuchiya, K., Yoshida, M., Hashizume, Y., & Oda, T. (2006). TDP-43 is a component of ubiquitin-positive tau-negative inclusions in frontotemporal lobar degeneration and amyotrophic lateral sclerosis. *Biochem Biophys Res Commun*, *351*(3), 602-611. https://doi.org/10.1016/j.bbrc.2006.10.093

Armstrong, G. A., & Drapeau, P. (2013). Loss and gain of FUS function impair neuromuscular synaptic transmission in a genetic model of ALS. *Hum Mol Genet*, *22*(21), 4282-4292. https://doi.org/10.1093/hmg/ddt278

Armstrong, G. A., Liao, M., You, Z., Lissouba, A., Chen, B. E., & Drapeau, P. (2016). Homology Directed Knockin of Point Mutations in the Zebrafish tardbp and fus Genes in ALS Using the CRISPR/Cas9 System. *PLoS One*, *11*(3), e0150188. https://doi.org/10.1371/journal.pone.0150188

Bang, J., Spina, S., & Miller, B. L. (2015). Frontotemporal dementia. *Lancet*, *386*(10004), 1672-1682. https://doi.org/10.1016/S0140-6736(15)00461-4

Baughn, M. W., Melamed, Z., Lopez-Erauskin, J., Beccari, M. S., Ling, K., Zuberi, A., Presa, M., Gonzalo-Gil, E., Maimon, R., Vazquez-Sanchez, S., Chaturvedi, S., Bravo-

Hernandez, M., Taupin, V., Moore, S., Artates, J. W., Acks, E., Ndayambaje, I. S., Agra de Almeida Quadros, A. R., Jafar-Nejad, P., . . . Cleveland, D. W. (2023). Mechanism of STMN2 cryptic splice-polyadenylation and its correction for TDP-43 proteinopathies. *Science*, *379*(6637), 1140-1149. https://doi.org/10.1126/science.abq5622

Beghi, E., Logroscino, G., Chio, A., Hardiman, O., Mitchell, D., Swingler, R., Traynor, B. J., & Consortium, E. (2006). The epidemiology of ALS and the role of population-based registries. *Biochim Biophys Acta*, *1762*(11-12), 1150-1157. https://doi.org/10.1016/j.bbadis.2006.09.008

Benarroch, E. (2021). What Is the Role of Stathmin-2 in Axonal Biology and Degeneration? *Neurology*, *97*(7), 330-333. https://doi.org/10.1212/WNL.0000000000012419

Bieche, I., Maucuer, A., Laurendeau, I., Lachkar, S., Spano, A. J., Frankfurter, A., Levy, P., Manceau, V., Sobel, A., Vidaud, M., & Curmi, P. A. (2003). Expression of stathmin family genes in human tissues: non-neural-restricted expression for SCLIP. *Genomics*, *81*(4), 400-410. https://doi.org/10.1016/s0888-7543(03)00031-4

Bose, P., Armstrong, G. A. B., & Drapeau, P. (2019). Neuromuscular junction abnormalities in a zebrafish loss-of-function model of TDP-43. *J Neurophysiol*, *121*(1), 285-297. https://doi.org/10.1152/jn.00265.2018

Boswell, C. W., & Ciruna, B. (2017). Understanding Idiopathic Scoliosis: A New Zebrafish School of Thought. *Trends Genet*, *33*(3), 183-196. https://doi.org/10.1016/j.tig.2017.01.001

Brown, R. H., Jr., & Al-Chalabi, A. (2017). Amyotrophic Lateral Sclerosis. *N Engl J Med*, *377*(16), 1602. https://doi.org/10.1056/NEJMc1710379

Buratti, E., & Baralle, F. E. (2001). Characterization and functional implications of the RNA binding properties of nuclear factor TDP-43, a novel splicing regulator of CFTR exon 9. *J Biol Chem*, *276*(39), 36337-36343. https://doi.org/10.1074/jbc.M104236200

Buratti, E., & Baralle, F. E. (2008). Multiple roles of TDP-43 in gene expression, splicing regulation, and human disease. *Front Biosci*, *13*, 867-878. https://doi.org/10.2741/2727

Burzynski, G. M., Delalande, J. M., & Shepherd, I. (2009). Characterization of spatial and temporal expression pattern of SCG10 during zebrafish development. *Gene Expr Patterns*, *9*(4), 231-237. https://doi.org/10.1016/j.gep.2008.12.010

Chauvin, S., & Sobel, A. (2015). Neuronal stathmins: a family of phosphoproteins cooperating for neuronal development, plasticity and regeneration. *Prog Neurobiol*, *126*, 1-18. https://doi.org/10.1016/j.pneurobio.2014.09.002

Cirulli, E. T., Lasseigne, B. N., Petrovski, S., Sapp, P. C., Dion, P. A., Leblond, C. S., Couthouis, J., Lu, Y. F., Wang, Q., Krueger, B. J., Ren, Z., Keebler, J., Han, Y., Levy, S. E., Boone, B. E., Wimbish, J. R., Waite, L. L., Jones, A. L., Carulli, J. P., . . . Goldstein, D. B. (2015). Exome sequencing in amyotrophic lateral sclerosis identifies risk genes and pathways. *Science*, *347*(6229), 1436-1441. https://doi.org/10.1126/science.aaa3650

Cruz, M. P. (2018). Edaravone (Radicava): A Novel Neuroprotective Agent for the Treatment of Amyotrophic Lateral Sclerosis. *P T*, *43*(1), 25-28. https://www.ncbi.nlm.nih.gov/pubmed/29290672

Curmi, P. A., Andersen, S. S., Lachkar, S., Gavet, O., Karsenti, E., Knossow, M., & Sobel, A. (1997). The stathmin/tubulin interaction in vitro. *J Biol Chem*, *272*(40), 25029-25036. https://doi.org/10.1074/jbc.272.40.25029

DeJesus-Hernandez, M., Mackenzie, I. R., Boeve, B. F., Boxer, A. L., Baker, M., Rutherford, N. J., Nicholson, A. M., Finch, N. A., Flynn, H., Adamson, J., Kouri, N., Wojtas, A., Sengdy, P., Hsiung, G. Y., Karydas, A., Seeley, W. W., Josephs, K. A., Coppola, G., Geschwind, D. H., . . . Rademakers, R. (2011). Expanded GGGGCC hexanucleotide repeat in noncoding region of C9ORF72 causes chromosome 9p-linked FTD and ALS. *Neuron*, *72*(2), 245-256. https://doi.org/10.1016/j.neuron.2011.09.011

Di Paolo, G., Lutjens, R., Pellier, V., Stimpson, S. A., Beuchat, M. H., Catsicas, S., & Grenningloh, G. (1997). Targeting of SCG10 to the area of the Golgi complex is mediated by its NH2-terminal region. *J Biol Chem*, *272*(8), 5175-5182. https://doi.org/10.1074/jbc.272.8.5175

Doronzio, P. N., Lattante, S., Marangi, G., Martello, F., Conte, A., Bisogni, G., Bernardo, D., Patanella, A. K., Meleo, E., Zollino, M., & Sabatelli, M. (2023). Analysis of STMN2 CA repeats in italian ALS patients shows no association. *Amyotroph Lateral Scler Frontotemporal Degener*, *24*(1-2), 152-154. https://doi.org/10.1080/21678421.2022.2102430

Draper, B. W., & Moens, C. B. (2009). A high-throughput method for zebrafish sperm cryopreservation and in vitro fertilization. *J Vis Exp*(29). https://doi.org/10.3791/1395

Erali, M., & Wittwer, C. T. (2010). High resolution melting analysis for gene scanning. *Methods*, *50*(4), 250-261. https://doi.org/10.1016/j.ymeth.2010.01.013

Gilbert, M. J., Zerulla, T. C., & Tierney, K. B. (2014). Zebrafish (Danio rerio) as a model for the study of aging and exercise: physical ability and trainability decrease with age. *Exp Gerontol*, *50*, 106-113. https://doi.org/10.1016/j.exger.2013.11.013

Goyal, N. A., Berry, J. D., Windebank, A., Staff, N. P., Maragakis, N. J., van den Berg, L. H., Genge, A., Miller, R., Baloh, R. H., Kern, R., Gothelf, Y., Lebovits, C., & Cudkowicz, M. (2020). Addressing heterogeneity in amyotrophic lateral sclerosis CLINICAL TRIALS. *Muscle Nerve*, *62*(2), 156-166. https://doi.org/10.1002/mus.26801

Grenningloh, G., Soehrman, S., Bondallaz, P., Ruchti, E., & Cadas, H. (2004). Role of the microtubule destabilizing proteins SCG10 and stathmin in neuronal growth. *J Neurobiol*, *58*(1), 60-69. https://doi.org/10.1002/neu.10279

Grima, N., Henden, L., Fearnley, L. G., Rowe, D. B., D'Silva, S., Pamphlett, R., Adams, L., Kiernan, M. C., Mazumder, S., Timmins, H. C., Zoing, M., Bahlo, M., Blair, I. P., & Williams, K. L. (2022). NEK1 and STMN2 short tandem repeat lengths are not associated with Australian amyotrophic lateral sclerosis risk. *Neurobiol Aging*, *116*, 92-95. https://doi.org/10.1016/j.neurobiolaging.2022.04.012

Guerra San Juan, I., Nash, L. A., Smith, K. S., Leyton-Jaimes, M. F., Qian, M., Klim, J. R., Limone, F., Dorr, A. B., Couto, A., Pintacuda, G., Joseph, B. J., Whisenant, D. E., Noble, C., Melnik, V., Potter, D., Holmes, A., Burberry, A., Verhage, M., & Eggan, K. (2022). Loss of mouse Stmn2 function causes motor neuropathy. *Neuron*, *110*(10), 1671-1688 e1676. https://doi.org/10.1016/j.neuron.2022.02.011

Gupta, K. K., Li, C., Duan, A., Alberico, E. O., Kim, O. V., Alber, M. S., & Goodson, H. V. (2013). Mechanism for the catastrophe-promoting activity of the microtubule destabilizer Op18/stathmin. *Proc Natl Acad Sci U S A*, *110*(51), 20449-20454. https://doi.org/10.1073/pnas.1309958110

Hebert, T., Drapeau, P., Pradier, L., & Dunn, R. J. (1994). Block of the rat brain IIA sodium channel alpha subunit by the neuroprotective drug riluzole. *Mol Pharmacol*, *45*(5), 1055-1060. https://www.ncbi.nlm.nih.gov/pubmed/8190096

Howe, K., Clark, M. D., Torroja, C. F., Torrance, J., Berthelot, C., Muffato, M., Collins, J. E., Humphray, S., McLaren, K., Matthews, L., McLaren, S., Sealy, I., Caccamo, M., Churcher, C., Scott, C., Barrett, J. C., Koch, R., Rauch, G. J., White, S., . . . Stemple, D. L. (2013). The zebrafish reference genome sequence and its relationship to the human genome. *Nature*, *496*(7446), 498-503. https://doi.org/10.1038/nature12111

Jao, L. E., Wente, S. R., & Chen, W. (2013). Efficient multiplex biallelic zebrafish genome editing using a CRISPR nuclease system. *Proc Natl Acad Sci U S A*, *110*(34), 13904-13909. https://doi.org/10.1073/pnas.1308335110

Johnson, S. A., Fang, T., De Marchi, F., Neel, D., Van Weehaeghe, D., Berry, J. D., & Paganoni, S. (2022). Pharmacotherapy for Amyotrophic Lateral Sclerosis: A Review of Approved and Upcoming Agents. *Drugs*, *82*(13), 1367-1388. https://doi.org/10.1007/s40265-022-01769-1

Kabashi, E., Champagne, N., Brustein, E., & Drapeau, P. (2010). In the swim of things: recent insights to neurogenetic disorders from zebrafish. *Trends Genet*, *26*(8), 373-381. https://doi.org/10.1016/j.tig.2010.05.004

Kiernan, M. C., Vucic, S., Cheah, B. C., Turner, M. R., Eisen, A., Hardiman, O., Burrell, J. R., & Zoing, M. C. (2011). Amyotrophic lateral sclerosis. *Lancet*, *377*(9769), 942-955. https://doi.org/10.1016/S0140-6736(10)61156-7

Klim, J. R., Williams, L. A., Limone, F., Guerra San Juan, I., Davis-Dusenbery, B. N., Mordes, D. A., Burberry, A., Steinbaugh, M. J., Gamage, K. K., Kirchner, R., Moccia, R., Cassel,

S. H., Chen, K., Wainger, B. J., Woolf, C. J., & Eggan, K. (2019). ALS-implicated protein TDP-43 sustains levels of STMN2, a mediator of motor neuron growth and repair. *Nat Neurosci*, *22*(2), 167-179. https://doi.org/10.1038/s41593-018-0300-4

Krus, K. L., Strickland, A., Yamada, Y., Devault, L., Schmidt, R. E., Bloom, A. J., Milbrandt, J., & DiAntonio, A. (2022). Loss of Stathmin-2, a hallmark of TDP-43-associated ALS, causes motor neuropathy. *Cell Rep*, *39*(13), 111001. https://doi.org/10.1016/j.celrep.2022.111001

Kwiatkowski, T. J., Jr., Bosco, D. A., Leclerc, A. L., Tamrazian, E., Vanderburg, C. R., Russ, C., Davis, A., Gilchrist, J., Kasarskis, E. J., Munsat, T., Valdmanis, P., Rouleau, G. A., Hosler, B. A., Cortelli, P., de Jong, P. J., Yoshinaga, Y., Haines, J. L., Pericak-Vance, M. A., Yan, J., . . . Brown, R. H., Jr. (2009). Mutations in the FUS/TLS gene on chromosome 16 cause familial amyotrophic lateral sclerosis. *Science*, *323*(5918), 1205-1208. https://doi.org/10.1126/science.1166066

Le Ber, I., De Septenville, A., Millecamps, S., Camuzat, A., Caroppo, P., Couratier, P., Blanc, F., Lacomblez, L., Sellal, F., Fleury, M. C., Meininger, V., Cazeneuve, C., Clot, F., Flabeau, O., LeGuern, E., Brice, A., French, C., & Genetic Research Network on, F. F.-A. (2015). TBK1 mutation frequencies in French frontotemporal dementia and amyotrophic lateral sclerosis cohorts. *Neurobiol Aging*, *36*(11), 3116 e3115-3116 e3118. https://doi.org/10.1016/j.neurobiolaging.2015.08.009

Lee, E. B., Lee, V. M., & Trojanowski, J. Q. (2011). Gains or losses: molecular mechanisms of TDP43-mediated neurodegeneration. *Nat Rev Neurosci*, *13*(1), 38-50. https://doi.org/10.1038/nrn3121

Li, Y., Tian, Y., Pei, X., Zheng, P., Miao, L., Li, L., Luo, C., Zhang, P., Jiang, B., Teng, J., Huang, N., & Chen, J. (2023). SCG10 is required for peripheral axon maintenance and regeneration in mice. *J Cell Sci*, *136*(12). https://doi.org/10.1242/jcs.260490

Ling, S. C., Polymenidou, M., & Cleveland, D. W. (2013). Converging mechanisms in ALS and FTD: disrupted RNA and protein homeostasis. *Neuron*, *79*(3), 416-438. https://doi.org/10.1016/j.neuron.2013.07.033

Livak, K. J., & Schmittgen, T. D. (2001). Analysis of relative gene expression data using real-time quantitative PCR and the 2(-Delta Delta C(T)) Method. *Methods*, *25*(4), 402-408. https://doi.org/10.1006/meth.2001.1262

Lopez-Erauskin, J., Bravo-Hernandez, M., Presa, M., Baughn, M. W., Melamed, Z., Beccari, M. S., Agra de Almeida Quadros, A. R., Arnold-Garcia, O., Zuberi, A., Ling, K., Platoshyn, O., Nino-Jara, E., Ndayambaje, I. S., McAlonis-Downes, M., Cabrera, L., Artates, J. W., Ryan, J., Hermann, A., Ravits, J., . . . Lagier-Tourenne, C. (2023). Stathmin-2 loss leads to neurofilament-dependent axonal collapse driving motor and sensory denervation. *Nat Neurosci*. https://doi.org/10.1038/s41593-023-01496-0

Manna, T., Grenningloh, G., Miller, H. P., & Wilson, L. (2007). Stathmin family protein SCG10 differentially regulates the plus and minus end dynamics of microtubules at steady state in vitro: implications for its role in neurite outgrowth. *Biochemistry*, *46*(11), 3543-3552. https://doi.org/10.1021/bi061819d

Masrori, P., & Van Damme, P. (2020). Amyotrophic lateral sclerosis: a clinical review. *Eur J Neurol*, *27*(10), 1918-1929. https://doi.org/10.1111/ene.14393

McCord, J. M., & Fridovich, I. (1969). Superoxide dismutase. An enzymic function for erythrocuprein (hemocuprein). *J Biol Chem*, *244*(22), 6049-6055. https://www.ncbi.nlm.nih.gov/pubmed/5389100

Melamed, Z., Lopez-Erauskin, J., Baughn, M. W., Zhang, O., Drenner, K., Sun, Y., Freyermuth, F., McMahon, M. A., Beccari, M. S., Artates, J. W., Ohkubo, T., Rodriguez, M., Lin, N., Wu, D., Bennett, C. F., Rigo, F., Da Cruz, S., Ravits, J., Lagier-Tourenne, C., & Cleveland, D. W. (2019). Premature polyadenylation-mediated loss of stathmin-2 is a hallmark of TDP-43-dependent neurodegeneration. *Nat Neurosci*, *22*(2), 180-190. https://doi.org/10.1038/s41593-018-0293-z

Miller, R. G., Mitchell, J. D., Lyon, M., & Moore, D. H. (2007). Riluzole for amyotrophic lateral sclerosis (ALS)/motor neuron disease (MND). *Cochrane Database Syst Rev*(1), CD001447. https://doi.org/10.1002/14651858.CD001447.pub2

Miller, T. M., Cudkowicz, M. E., Genge, A., Shaw, P. J., Sobue, G., Bucelli, R. C., Chio, A., Van Damme, P., Ludolph, A. C., Glass, J. D., Andrews, J. A., Babu, S., Benatar, M., McDermott, C. J., Cochrane, T., Chary, S., Chew, S., Zhu, H., Wu, F., . . . Group, O. L. E. W. (2022). Trial of Antisense Oligonucleotide Tofersen for SOD1 ALS. *N Engl J Med*, *387*(12), 1099-1110. https://doi.org/10.1056/NEJMoa2204705

Mitchison, T., & Kirschner, M. (1984). Dynamic instability of microtubule growth. *Nature*, *312*(5991), 237-242. https://doi.org/10.1038/312237a0

Moreno-Mateos, M. A., Vejnar, C. E., Beaudoin, J. D., Fernandez, J. P., Mis, E. K., Khokha, M. K., & Giraldez, A. J. (2015). CRISPRscan: designing highly efficient sgRNAs for CRISPR-Cas9 targeting in vivo. *Nat Methods*, *12*(10), 982-988. https://doi.org/10.1038/nmeth.3543

Munoz-Montecinos, C., Romero, A., Sepulveda, V., Vira, M. A., Fehrmann-Cartes, K., Marcellini, S., Aguilera, F., Caprile, T., & Fuentes, R. (2021). Turning the Curve Into Straight: Phenogenetics of the Spine Morphology and Coordinate Maintenance in the Zebrafish. *Front Cell Dev Biol*, *9*, 801652. https://doi.org/10.3389/fcell.2021.801652

Neumann, M., Sampathu, D. M., Kwong, L. K., Truax, A. C., Micsenyi, M. C., Chou, T. T., Bruce, J., Schuck, T., Grossman, M., Clark, C. M., McCluskey, L. F., Miller, B. L., Masliah, E., Mackenzie, I. R., Feldman, H., Feiden, W., Kretzschmar, H. A., Trojanowski, J. Q., & Lee, V. M. (2006). Ubiquitinated TDP-43 in frontotemporal lobar degeneration and amyotrophic lateral sclerosis. *Science*, *314*(5796), 130-133. https://doi.org/10.1126/science.1134108

Orsini, M., Oliveira, A. B., Nascimento, O. J., Reis, C. H., Leite, M. A., de Souza, J. A., Pupe, C., de Souza, O. G., Bastos, V. H., de Freitas, M. R., Teixeira, S., Bruno, C., Davidovich, E., & Smidt, B. (2015). Amyotrophic Lateral Sclerosis: New Perpectives and Update. *Neurol Int*, *7*(2), 5885. https://doi.org/10.4081/ni.2015.5885

Oskarsson, B., Gendron, T. F., & Staff, N. P. (2018). Amyotrophic Lateral Sclerosis: An Update for 2018. *Mayo Clin Proc*, *93*(11), 1617-1628. https://doi.org/10.1016/j.mayocp.2018.04.007

Paganoni, S., Hendrix, S., Dickson, S. P., Knowlton, N., Berry, J. D., Elliott, M. A., Maiser, S., Karam, C., Caress, J. B., Owegi, M. A., Quick, A., Wymer, J., Goutman, S. A., Heitzman, D., Heiman-Patterson, T. D., Jackson, C., Quinn, C., Rothstein, J. D., Kasarskis, E. J., . . . Cudkowicz, M. (2022). Effect of sodium phenylbutyrate/taurursodiol on tracheostomy/ventilation-free survival and hospitalisation in amyotrophic lateral

sclerosis: long-term results from the CENTAUR trial. *J Neurol Neurosurg Psychiatry*, *93*(8), 871-875. https://doi.org/10.1136/jnnp-2022-329024

Paganoni, S., Hendrix, S., Dickson, S. P., Knowlton, N., Macklin, E. A., Berry, J. D., Elliott, M. A., Maiser, S., Karam, C., Caress, J. B., Owegi, M. A., Quick, A., Wymer, J., Goutman, S. A., Heitzman, D., Heiman-Patterson, T. D., Jackson, C. E., Quinn, C., Rothstein, J. D., . . . Cudkowicz, M. E. (2021). Long-term survival of participants in the CENTAUR trial of sodium phenylbutyrate-taurursodiol in amyotrophic lateral sclerosis. *Muscle Nerve*, *63*(1), 31-39. https://doi.org/10.1002/mus.27091

Paganoni, S., Macklin, E. A., Hendrix, S., Berry, J. D., Elliott, M. A., Maiser, S., Karam, C., Caress, J. B., Owegi, M. A., Quick, A., Wymer, J., Goutman, S. A., Heitzman, D., Heiman-Patterson, T., Jackson, C. E., Quinn, C., Rothstein, J. D., Kasarskis, E. J., Katz, J., . . . Cudkowicz, M. E. (2020). Trial of Sodium Phenylbutyrate-Taurursodiol for Amyotrophic Lateral Sclerosis. *N Engl J Med*, *383*(10), 919-930. https://doi.org/10.1056/NEJMoa1916945

Pasinelli, P., & Brown, R. H. (2006). Molecular biology of amyotrophic lateral sclerosis: insights from genetics. *Nat Rev Neurosci*, *7*(9), 710-723. https://doi.org/10.1038/nrn1971

Patton, E. E., Zon, L. I., & Langenau, D. M. (2021). Zebrafish disease models in drug discovery: from preclinical modelling to clinical trials. *Nat Rev Drug Discov*, *20*(8), 611-628. https://doi.org/10.1038/s41573-021-00210-8

Renton, A. E., Majounie, E., Waite, A., Simon-Sanchez, J., Rollinson, S., Gibbs, J. R., Schymick, J. C., Laaksovirta, H., van Swieten, J. C., Myllykangas, L., Kalimo, H., Paetau, A., Abramzon, Y., Remes, A. M., Kaganovich, A., Scholz, S. W., Duckworth, J., Ding, J., Harmer, D. W., . . . Traynor, B. J. (2011). A hexanucleotide repeat expansion in

C9ORF72 is the cause of chromosome 9p21-linked ALS-FTD. *Neuron*, *72*(2), 257-268. https://doi.org/10.1016/j.neuron.2011.09.010

Ringholz, G. M., Appel, S. H., Bradshaw, M., Cooke, N. A., Mosnik, D. M., & Schulz, P. E. (2005). Prevalence and patterns of cognitive impairment in sporadic ALS. *Neurology*, *65*(4), 586-590. https://doi.org/10.1212/01.wnl.0000172911.39167.b6

Rosen, D. R., Siddique, T., Patterson, D., Figlewicz, D. A., Sapp, P., Hentati, A., Donaldson, D., Goto, J., O'Regan, J. P., Deng, H. X., & et al. (1993). Mutations in Cu/Zn superoxide dismutase gene are associated with familial amyotrophic lateral sclerosis. *Nature*, *362*(6415), 59-62. https://doi.org/10.1038/362059a0

Ross, J. P., Akcimen, F., Liao, C., Spiegelman, D., Weisburd, B., Dupre, N., Dion, P. A., Rouleau, G. A., & Farhan, S. M. K. (2022). Questioning the Association of the STMN2 Dinucleotide Repeat With Amyotrophic Lateral Sclerosis. *Neurol Genet*, *8*(4), e678. https://doi.org/10.1212/NXG.0000000000000678

Seda, M., Crespo, B., Corcelli, M., Osborn, D. P., & Jenkins, D. (2023). A CRISPR/Cas9-generated mutation in the zebrafish orthologue of PPP2R3B causes idiopathic scoliosis. *Sci Rep*, *13*(1), 6783. https://doi.org/10.1038/s41598-023-33589-y

Shin, J. E., Miller, B. R., Babetto, E., Cho, Y., Sasaki, Y., Qayum, S., Russler, E. V., Cavalli, V., Milbrandt, J., & DiAntonio, A. (2012). SCG10 is a JNK target in the axonal degeneration pathway. *Proc Natl Acad Sci U S A*, *109*(52), E3696-3705. https://doi.org/10.1073/pnas.1216204109

Smeyers, J., Banchi, E. G., & Latouche, M. (2021). C9ORF72: What It Is, What It Does, and Why It Matters. *Front Cell Neurosci*, *15*, 661447. https://doi.org/10.3389/fncel.2021.661447

Stein, R., Mori, N., Matthews, K., Lo, L. C., & Anderson, D. J. (1988). The NGF-inducible SCG10 mRNA encodes a novel membrane-bound protein present in growth cones and abundant in developing neurons. *Neuron*, *1*(6), 463-476. https://doi.org/10.1016/0896-6273(88)90177-8

Sur, A., Wang, Y., Capar, P., Margolin, G., Prochaska, M. K., & Farrell, J. A. (2023). Single-cell analysis of shared signatures and transcriptional diversity during zebrafish development. *Dev Cell*. https://doi.org/10.1016/j.devcel.2023.11.001

Tararuk, T., Ostman, N., Li, W., Bjorkblom, B., Padzik, A., Zdrojewska, J., Hongisto, V., Herdegen, T., Konopka, W., Courtney, M. J., & Coffey, E. T. (2006). JNK1 phosphorylation of SCG10 determines microtubule dynamics and axodendritic length. *J Cell Biol*, *173*(2), 265-277. https://doi.org/10.1083/jcb.200511055

Taylor, J. P., Brown, R. H., Jr., & Cleveland, D. W. (2016). Decoding ALS: from genes to mechanism. *Nature*, *539*(7628), 197-206. https://doi.org/10.1038/nature20413

Theunissen, F., Anderton, R. S., Mastaglia, F. L., Flynn, L. L., Winter, S. J., James, I., Bedlack, R., Hodgetts, S., Fletcher, S., Wilton, S. D., Laing, N. G., MacShane, M., Needham, M., Saunders, A., Mackay-Sim, A., Melamed, Z., Ravits, J., Cleveland, D. W., & Akkari, P. A. (2021). Novel STMN2 Variant Linked to Amyotrophic Lateral Sclerosis Risk and Clinical Phenotype. *Front Aging Neurosci*, *13*, 658226. https://doi.org/10.3389/fnagi.2021.658226

Vance, C., Rogelj, B., Hortobagyi, T., De Vos, K. J., Nishimura, A. L., Sreedharan, J., Hu, X., Smith, B., Ruddy, D., Wright, P., Ganesalingam, J., Williams, K. L., Tripathi, V., Al-Saraj, S., Al-Chalabi, A., Leigh, P. N., Blair, I. P., Nicholson, G., de Belleroche, J., . . . Shaw, C. E. (2009). Mutations in FUS, an RNA processing protein, cause familial

amyotrophic lateral sclerosis type 6. *Science*, *323*(5918), 1208-1211. https://doi.org/10.1126/science.1165942

Varidaki, A., Hong, Y., & Coffey, E. T. (2018). Repositioning Microtubule Stabilizing Drugs for Brain Disorders. *Front Cell Neurosci*, *12*, 226. https://doi.org/10.3389/fncel.2018.00226

Vejnar, C. E., Moreno-Mateos, M. A., Cifuentes, D., Bazzini, A. A., & Giraldez, A. J. (2016). Optimized CRISPR-Cas9 System for Genome Editing in Zebrafish. *Cold Spring Harb Protoc*, *2016*(10). https://doi.org/10.1101/pdb.prot086850

Wang, H., Guan, L., & Deng, M. (2023). Recent progress of the genetics of amyotrophic lateral sclerosis and challenges of gene therapy. *Front Neurosci*, *17*, 1170996. https://doi.org/10.3389/fnins.2023.1170996

Westerfield, M. (1995). *The zebrafish book : a guide for the laboratory use of zebrafish (danio rerio)*. M. Westerfield?

Writing, G., & Edaravone, A. L. S. S. G. (2017). Safety and efficacy of edaravone in well defined patients with amyotrophic lateral sclerosis: a randomised, double-blind, placebo-controlled trial. *Lancet Neurol*, *16*(7), 505-512. https://doi.org/10.1016/S1474-4422(17)30115-1